ELEMENTA
Science of the Anthropocene

Campbell, K, et al. 2022. Net heterotrophy in High Arctic first-year and multi-year spring sea ice. *Elem Sci Anth*, 10: 1. DOI: https://doi.org/10.1525/elementa.2021.00040

RESEARCH ARTICLE

Net heterotrophy in High Arctic first-year and multi-year spring sea ice

Karley Campbell[1,2,*], B. A. Lange[3,4], J. C. Landy[2,5], C. Katlein[6], M. Nicolaus[6], P. Anhaus[6], I. Matero[6], R. Gradinger[1], J. Charette[4], S. Duerksen[4,7], P. Tremblay[4], S. Rysgaard[8,9], M. Tranter[2], C. Haas[6,10], and C. Michel[4,7]

The net productivity of sea ice is determined by the physical and geochemical characteristics of the ice–ocean system and the activity of organisms inhabiting the ice. Differences in habitat suitability between first-year and multi-year sea ice can affect the ice algal community composition and acclimation state, introducing considerable variability to primary production within each ice type. In this study, we characterized the biogeochemical variability between adjacent first-year and multi-year sea ice floes in the Lincoln Sea of the Canadian High Arctic, during the May 2018 Multidisciplinary Arctic Program—Last Ice sampling campaign. Combining measurements of transmitted irradiance from a remotely operated underwater vehicle with laboratory-based oxygen optode incubations, this work shows widespread heterotrophy (net oxygen uptake) in the bottom 10 cm of both ice types, particularly in thick multi-year ice (>2.4 m) and early morning of the 24-h day. Algal acclimation state and species composition varied between ice types despite similar net community production due to widespread light and nutrient limitation. The first-year ice algal community was increasingly dominated over spring by the potentially toxin-producing genus *Pseudonitzschia* that was acclimated to high and variable light conditions characteristic of a thinner ice habitat with mobile snow cover. In comparison, the multi-year ice harbored more shade-acclimated algae of mixed composition. This work highlights the potential for heterotrophy in sea ice habitats of the High Arctic, including first measurements of such O_2-uptake in multi-year ice floes. Observed differences in photophysiology between algae of these sea ice types suggests that a shift toward higher light availability and a younger sea ice cover with climate change does not necessarily result in a more productive system. Instead, it may favor future sea ice algal communities of different species composition, with lower photosynthetic potential but greater resilience to stronger and more variable light conditions.

Keywords: Heterotrophy, Net community production, Sea ice, Arctic

1. Introduction

Algae inhabiting sea ice account for a significant portion of total primary production in the Arctic marine system, particularly in the High Arctic (e.g., Arctic Basin) where the contribution from multi-year sea ice (MYI; see Text S1 for list of abbreviations) algae to total production can be as high as 60% (Gosselin et al., 1997; Fernández-Méndez et al., 2015). Diatoms that dominate spring ice algal blooms also provide a concentrated food resource for sea ice and pelagic herbivores when phytoplankton growth is limited (Michel et al., 1996; Leu et al., 2015) and for benthic herbivores following diatom export to the ocean floor, which is especially evident during the period of bloom termination (Fortier et al., 2002). Together with heterotrophic bacteria, the productivity of sea ice algae helps to determine the role of sea ice as a sink or source of CO_2 in the global carbon cycle (Moreau et al., 2016; Lannuzel et al., 2020) and thus our understanding of how the

[1] Department of Arctic and Marine Biology, UiT The Arctic University of Norway, Tromsø, Norway
[2] Bristol Glaciology Centre, School of Geographical Sciences, University of Bristol, Bristol, United Kingdom
[3] Norwegian Polar Institute, Tromsø, Norway
[4] Fisheries and Oceans Canada, Freshwater Institute, Winnipeg, MB, Canada
[5] Department of Physics and Technology, UiT The Arctic University of Norway, Tromsø, Norway
[6] Alfred Wegener Institute Helmholtz Centre for Polar and Marine Research, Bremerhaven, Germany
[7] Fisheries and Oceans Canada, Bedford Institute of Oceanography, Dartmouth, NS, Canada
[8] Centre for Earth Observation Science, University of Manitoba, Winnipeg, MB, Canada
[9] Arctic Research Centre, Department of Bioscience, University of Aarhus, Aarhus, Denmark
[10] Department of Earth and Space Sciences, York University, Toronto, Canada

* Corresponding author:
Email: karley.l.campbell@uit.no

ice-covered Arctic Ocean functions to capture or contribute to rising atmospheric concentrations of CO_2.

At the timing of peak ice cover in winter, first-year sea ice (FYI) covers more than 70% of the Arctic Ocean and is a seasonally prominent feature of continental shelf seas (Tschudi et al., 2020). Over recent decades, atmospheric and ocean-related warming has increased the dominance of FYI in the High Arctic, as MYI has been lost by melt, breakup, or export from central basins of the Arctic Ocean (Maslanik et al., 2007; Kwok, 2018). FYI is typically characterized by a relatively uniform thickness within a given region and wind-drifted snow cover (Iacozza and Barber, 1999; Webster et al., 2018), with the latter predominantly controlling the magnitude of light transmission through the snow and sea ice to the ocean below (Grenfell and Maykut, 1977; Perovich, 1990; Nicolaus et al., 2012; Katlein et al., 2019). In comparison, annual melt and freeze cycles create substantial heterogeneity across the MYI cover, with surface elevations (hummocks, pressure ridges) and depressions (non-hummocked ice and melt ponds) that either reduce or enhance, respectively, the accumulation of light-attenuating snow (Iacozza and Barber, 1999; Lange et al., 2017).

The production of sea ice algae depends largely on the availability of light and nutrients while indirectly being influenced by the species composition of the ice algal community (Campbell et al., 2015; Campbell et al., 2018). The majority of ice algal studies have focused on coastal FYI, while far fewer have documented the abundance and productivity of cells in the older MYI habitats of the central Arctic Ocean (e.g., Gosselin et al., 1997; Gradinger, 1999; Schünemann and Werner, 2005; Fernández-Méndez et al., 2015). The magnitudes of the sea ice algal blooms in MYI compared to FYI are thought to be restricted by thicker snow and the ice thickness, which reduce light transmission (Nicolaus et al., 2012; Wang et al., 2014; Katlein et al., 2015). However, hummock features have been undersampled in biogeochemical studies, leading to a potential underestimation of the contribution of MYI algae to total marine production (Lange et al., 2015; Lange et al., 2017). This undersampling is despite the possibility that hummocks have a greater potential for photosynthetic activity due to their thinner or negligible snow cover in comparison to surrounding non-hummocked ice (Lange et al., 2015; Lange et al., 2017; Lange et al., 2019).

Differences in light intensity within and between the bottom of sea ice habitats can lead to variations in species composition, photophysiology, and production of ice algal communities. Studies of ridged and smooth FYI have shown that species of centric diatoms may dominate over pennates under high light conditions, which can occur on the upward-facing ridge subsurfaces (Fernández-Méndez et al., 2018), under thin snow covers, or during the late spring season (Campbell et al., 2018). The acclimation response of sea ice algal photophysiology to light availability is less clear. Seasonal increases in downwelling irradiance have been shown to cause an increase in algal maximum photosynthetic rate relative to chlorophyll *a* (chl *a*; P_m^B; i.e., theoretical upper limit of production) and a decrease in photoinhibition over spring FYI blooms (Michel et al., 1988; Campbell et al., 2016). However, no significant differences were found in P_m^B between locations of differing snow depths (Campbell et al., 2016). A limited number of photophysiological measurements have been made for algae inhabiting MYI, but studies such as Fernández-Méndez et al. (2015) have suggested comparable rates of P_m^B between FYI and MYI, with potentially greater photosynthetic efficiencies relative to chl *a* (α^B; i.e., capacity for light-limited production relative to light absorption) in MYI. However, in such studies, the focus was on late-summer (post-bloom) communities of FYI and MYI floes from geographically distanced regions of the Arctic.

In addition to differences in the amount of light transmitted through sea ice as a result of snow and ice thickness, the stability of the light environment differs between FYI and MYI as a result of surface topography. Higher spatial variability is found under level FYI where snow drifts migrate more easily across the ice surface (Iacozza and Barber, 1999) versus MYI where snow remains effectively trapped between hummock features (Lange et al., 2019). The uneven distribution of snow and thus light available for algal growth, particularly in FYI, results in significant spatial variability in ice algal biomass (Cimoli et al., 2017; Castellani et al., 2020), which makes representative sampling of ice algal abundance and production by discrete sampling methods like ice coring difficult. Methodological developments that remotely estimate ice algal abundance by optical methods have increased the potential to fully capture the patchy distribution of algae along the sea ice–ocean interface (e.g., Katlein et al., 2017; Castellani et al., 2020; Matthes et al., 2020). These developments include the use of remotely operated underwater vehicles (ROVs) and manual deployment of underice sensors. However, in terms of areal coverage, these applications have been limited largely to the subfloe scale. Furthermore, without the modeling of algal photophysiology from photosynthesis-irradiance (*P–E*) style incubations, primary production currently cannot be estimated from such remote sensing platforms. An alternative to estimating primary production, as in a majority of studies, relies upon a radioisotope tracer to estimate the rate of carbon fixation by photosynthesis (i.e., ^{14}C) for samples of ice algae collected from a given point (ice core) location, after the sample has been removed from the sea ice environment. Measurements of production, the balance between respiration and photosynthesis at the community level (Rysgaard and Glud, 2004; Rysgaard et al., 2008), and algal stress (Kennedy et al., 2020) can also be assessed using in situ or in vivo O_2-based technologies. These studies have shown net heterotrophic conditions (net O_2 uptake) during the initial spring bloom period in FYI due to high respiration (Campbell et al., 2017). Such O_2-based measurements are not currently available for High Arctic FYI or MYI habitats, which limits our understanding of net productivity across a significant portion of the Arctic.

In this study, we contrast biogeochemical properties of sea ice algae within adjacent FYI and MYI floes in the Lincoln Sea of the Canadian High Arctic during the

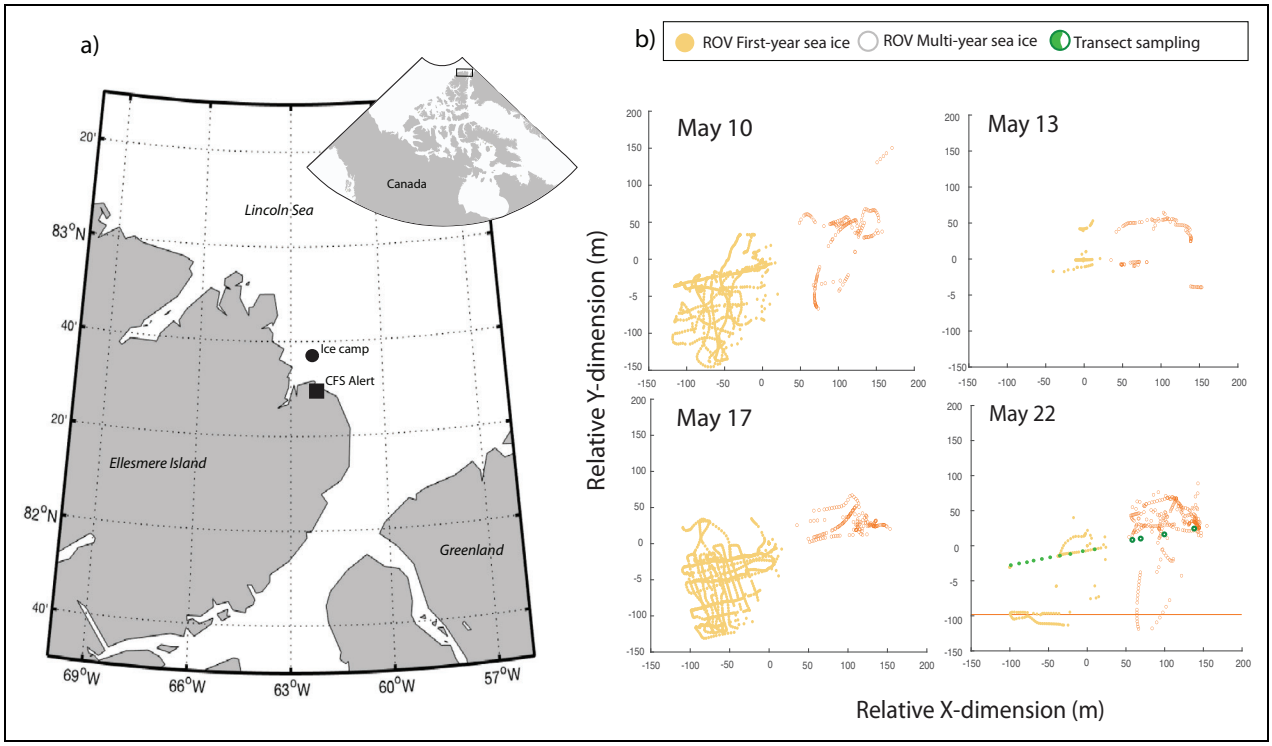

Figure 1. Illustration of study area in the Lincoln Sea during spring 2018. (a) Position of the ice camp offshore from the Canadian Forces Station Alert and (b) spatial grid of remotely operated vehicle measurements taken at the ice camp under first-year sea ice (FYI; yellow) and multi-year sea ice (MYI; gray) on May 10, 13, 17, and 22. Positions of the transect locations of ice collection where samples were taken on May 23 (green) are shown on the May 22 ROV surface for FYI (small green circles, $n = 10$) and MYI (bold green circles, $n = 4$). DOI: https://doi.org/10.1525/elementa.2021.00040.f1

2018 Multidisciplinary Arctic Program (MAP)—Last Ice study. This contrast includes biogeochemical characteristics and O_2-based models of photophysiology from core-based samples of both FYI and MYI. The discrete observations are scaled-up using optical measurements from an ROV to estimate chl *a* biomass and net community production (NCP) across ice-floe scales in the study region. From these results, we quantify the productivity of both FYI and MYI in the Canadian High Arctic, offering new insight on the potential ecosystem impacts of rapidly declining Arctic MYI. We further differentiate between comparatively thin (e.g., non-hummocked; MYI_{thin}) and thick (hummocked or ridged; MYI_{thick}) MYI sea ice to examine the potential variability within this understudied ice habitat. Through this work, the hypothesis that algal communities of bottom sea ice in the Lincoln Sea exhibit a net heterotrophic phase of production during the spring regardless of ice type is evaluated.

2. Materials and methods

2.1. Study site and sample collection

This study was part of the MAP—Last ice sampling campaign in the Lincoln Sea (82.576°N 62.471°W), located offshore from the Canadian Forces Station Alert (**Figure 1a**). Samples were collected from adjacent snow-covered FYI and MYI floes prior to spring melt (May 7–23, 2018; Figure S1) when atmospheric temperatures remained below freezing. Due to their proximity, sample sites on both floes had experienced the same meteorological and oceanographic conditions (Lange et al., 2019).

The bottom 10 cm of sea ice cores were collected on May 23 from 14 locations along a 240-m transect spanning both FYI and MYI floes, using a 9-cm diameter Mark II ice coring system from Kovacs Enterprise LLC. These transect-based ice samples were collected from under a range of snow covers and were melted over 36–48 h without the addition of filtered seawater (FSW) for subsequent analysis of chl *a* (Lange et al., 2019) and exopolymeric substances (EPS). Separately, FYI and MYI sites previously not visited (i.e., undisturbed) were cored near the transect on May 4 (FYI), 7 (MYI), and 23 (FYI and MYI) for incubation and taxonomic analysis, as well as on May 11 (MYI), 15 (FYI), and 19 (FYI and MYI) for taxonomy only (**Table 1**). Here, the bottom 10 cm of 7 sea ice cores per ice type were pooled together prior to 24 h of unbuffered melt to provide an averaged sample that accounts for potential variability between cores. The bottom 10 cm section of ice was targeted for sample collection, as initial analysis of both FYI and MYI on May 7 showed that it contained the vast majority (>95%) of chl *a* (Figure S2).

2.2. Laboratory analyses

2.2.1. Transect chl *a* and EPS

The concentrations of chl *a* (mg m^{-2}) and particulate EPS (mg ml^{-1}) were determined for ice cores at transect sample locations based on subsamples collected immediately

Table 1. Average values ± standard deviation for ice thickness (H_I), freeboard (F_b) and snow thickness (H_S) for first-year (FYI) and multi-year (MYI) sea ice by date of ice core collection, along with which pooled ice core samples were used for photosynthesis-irradiance (*P–E*) incubations and taxonomic analyses (taxa). DOI: https://doi.org/10.1525/elementa.2021.00040.t1

	FYI			MYI				
Date (May, 2018)	H_I (cm)	F_b (cm)	H_S (cm)	H_I (cm)	F_b (cm)	H_S (cm)	*P–E*	Taxa
4	158 ± 2	11 ± 1	10 ± 1	—[a]	—	—	FYI	—
7	—	—	—	324 ± 21	34 ± 8	24 ± 5	MYI	MYI
11	167 ± 1	11 ± 1	8 ± 1	353 ± 20	51 ± 2	5 ± 1	—	FYI and MYI
15	166 ± 2	13 ± 0	4 ± 1	—	—	—	—	FYI
19	176 ± 4	15 ± 1	3 ± 1	384 ± 7	61 ± 3	4 ± 2	—	FYI and MYI
23[b]	176 ± 1	13 ± 1	16 ± 2	455 ± 2	68 ± 2	4 ± 1	FYI and MYI	FYI and MYI
Study average	169 ± 7	13 ± 2	8 ± 5	383 ± 51	55 ± 13	8 ± 8	—	—

[a]Emdashes indicate dates when data were not collected.

[b]Ice cores collected from transect locations on May 23 are summarized in the text and detailed in Lange et al. (2019).

after ice samples were melted. Average chl *a* was assessed by filtration of pseudoduplicate samples onto GF/F (Whatman) filters and extraction of pigments in 90% acetone for 18–24 h, followed by measurements of fluorescence before and after acidification (Turner Designs 10AU fluorometer; Parsons et al., 1984). Particulate EPS samples were collected onto 0.4 μm polycarbonate filters (Millipore) and stored at −20°C until processing within 6 months by the phenol-sulfuric acid method using glucose as a calibration standard (Dubois et al., 1956). Here, carbohydrates of filter samples were extracted in the phenol-sulfuric acid solution for 24 h before measurement of absorption at 490 nm via spectrophotometer (Agilent Cary 60). Hereafter, these measurements of glucose equivalence are reported simply as EPS (mg ml^{-1}) of melted sea ice.

2.2.2. Oxygen optode incubations and taxonomy

NCP was determined on two occasions over the spring sample period for both FYI (May 4 and 23) and MYI (May 7 and 23), using the oxygen optode method of Campbell et al. (2016), modified to accommodate six 750-mL incubation bottles. Briefly, this setup incubates the meltwater of pooled ice core samples in overfilled and gas-tight borosilicate glass bottles (Wheaton), equipped with continuously logging Firesting oxygen optodes and magnetic stirring. Bottles were arranged across a range of light intensities from zero to 230 μmol m^2 s^{-1} in a temperature-controlled chamber, from which the relative change in dissolved oxygen over a 36-h incubation period was calculated. To minimize the influence of grazing activity on NCP and prevent bubble formation, samples were filtered through a 350-μm Nitex screen during the filling of incubation bottles with a peristaltic pump.

Chlorophyll *a* was sampled from these pooled core samples immediately after ice melt and prior to setup of optode incubations (T_0). Pseudo-duplicate samples were filtered onto 25-mm GF/F filters (Whatman) that were stored at −80°C for approximately 6 months. The average concentration of chl *a* (μg L^{-1}) was subsequently determined using before and after acidification fluorescence readings for each filter (Turner Designs Trilogy Fluorometer; Parsons et al., 1984), following the extraction of pigments into 90% acetone for 18–24 h. Samples were sonicated and vortexed prior to extraction and measurements of fluorescence, respectively, to ensure maximum recovery of pigments.

Pooled ice cores were also subsampled on May 11, 15, 19, and 23 (FYI) and May 7, 11, 19, and 23 (MYI) for analysis of community composition. Dates overlapping with the optode incubations described above represent production and taxonomy measurements from the same sample. Here, 20-mL subsamples from the pooled ice cores were fixed with acidic Lugol's solution (Parsons et al., 1984) for cell enumeration, morphological similarity (i.e., functional group), and where possible taxonomic identification. These samples were analyzed at 400× magnification within 1 year of collection using an inverted light microscope (Nikon) and the protocol outlined in Campbell et al. (2018). This method includes enumeration of a minimum of 400 cells over 3 transects. Subsamples of pooled meltwater were also taken on days of optode incubation (except for May 4, FYI) for analysis of inorganic nutrients. These subsamples were collected by filtering the ice meltwater through precombusted GF/F filters (Whatman). The filtrate was stored at −20°C and later analyzed on a LaChat QuikChem 8500 series 2 flow injection analyzer (QuikChem Method 31-114-27-1-D) for nitrate (NO_3) and nitrite (NO_2), phosphate (PO_4), as well as silicic acid ($Si(OH)_4$) according to Strickland and Parsons (1972). The uptake of nitrogen (nitrate + nitrite) and phosphate over the hourly duration of optode incubations (μmol L^{-1} h^{-1}) was calculated as:

$$\text{Uptake} = (N_n - N_0)/h, \quad (1)$$

where duplicate nutrient concentrations were sampled directly from the pooled ice cores (N_0) and again from the mixed volume of all incubation bottles immediately after termination of the optode experiment (N_n). This calculation was not made for $Si(OH)_4$ due to contamination from the silicate glass incubation bottle over the duration of incubation.

2.2.3. Modeling of photophysiology

P–E relationships were calculated from optode incubations as chl *a*-specific (^{B}) NCP versus incubation light intensity. The *P–E* relationship for each ice type (May 4, FYI; May 7, MYI; and May 23, FYI and MYI; **Table 1**) was modeled using the exponential equation of Platt et al. (1980) modified by Arrigo et al. (2010) without or with photoinhibition ($e^{\frac{-\beta E}{P_m}}$), depending on whether it was observed:

$$NCP = P_s^B(1 - e^{\frac{-\alpha}{P_s^B}})e^{\frac{-\beta E}{P_s^B}} - P_0^B. \quad (2)$$

Subsequent calculation of average photosynthetic parameters relative to chl *a* include P_s^B, maximum photosynthetic rate (μmol O_2 μg chl a^{-1} h^{-1}) in the absence of photoinhibition; α^B, photosynthetic efficiency (μmol O_2 μg chl a^{-1} h^{-1} [μmol photons m^{-2} s^{-1}]$^{-1}$); P_0^B, production at zero irradiance (μmol O_2 μg chl a^{-1} h^{-1}); I_c, irradiance where the rate of photosynthesis is balanced by respiration ($I_c = P_0^B/\alpha^B$) (μmol photons m^{-2} s^{-1}); I_s, the photoacclimation parameter ($I_s = P_s^B/\alpha^B$) (μmol photons m^{-2} s^{-1}); and where applicable b^B (β/P_s^B), slope of photoinhibition portion of *P–E* curve (μmol O_2 μg chl a^{-1} h^{-1} [μmol photons m^{-2} s^{-1}]$^{-1}$); I_β, index of photoinhibition (μmol photons m^{-2} s^{-1}) and P_m^B, realized production in the presence of photoinhibition (μmol O_2 μg chl a^{-1} h^{-1}; Platt et al., 1980; Cota and Smith, 1991). The *P–E* function for each sea ice type was calculated based on the two sets of incubations measured per ice type.

2.3. Measurements from the ROV

Underice surveys of spectral (350–950 nm) transmitted irradiance ($I_{(z,\ \lambda)}$) were conducted using a TriOs Ramses hyperspectral radiometer (Advanced Cosine Collector-VIS) mounted on an Ocean Modules M500 ROV (Nicolaus et al., 2010). Surveys on May 23 followed the transect described above, immediately prior to the collection of ice cores. Additional surveys on May 10, 13, 17, and 22 followed a more randomized or grid-like dive path of greater spatial coverage over an area of approximately 22,500 m^2 (150 × 150 m; **Figure 1**). Specific operational configurations of the ROV are described in Katlein et al. (2017), and information on sensor footprints has been discussed in Lange et al. (2016; Lange et al., 2017). Transmittance ($T_{(z,\ \lambda)}$; %) was calculated from instantaneous measurements of $I_{(z,\ \lambda)}$ and surface downwelling irradiance $I_{(0,\ \lambda)}$ from another TriOs Ramses hyperspectral radiometer (350–950 nm) positioned 1 m above the nearby snow-covered ice surface. The measurements of $T_{(z,\ \lambda)}$ and $I_{(0,\ \lambda)}$ were also integrated over the biologically relevant wavelengths of photosynthetically active radiation (PAR; 400–700 nm), hereafter reported as point measurements of $T_{(z,\ PAR)}$ and hourly averages of $I_{(0,\ PAR)}$, respectively. The distance upward to the sea ice base from the ROV (D_{ice}; m) was recorded by a sonar altimeter (PA200, Tritech, UK) mounted on the ROV, and together with the ROV depth was used to calculate sea ice draft (SID). To ensure accuracy of measurements, data were filtered to remove measurements where the ROV was significantly tilted ($\pm 10°$) or deeper than 5 m below the sea ice–ocean interface (Nicolaus et al., 2013; Katlein et al., 2017).

We distinguish between thin and thick MYI features (Figure S1) in our study using a simple threshold SID of 2.4 m, the average SID from all ROV dives under MYI (MYI_{avg}; **Table 2**). Data for MYI_{thin} are hereafter defined as measurements with corresponding SID < 2.4 m, and MYI_{thick} as locations with SID ≥ 2.4 m. The standard deviation of MYI SID from all ROV dives was 0.7 m (**Table 2**).

2.3.1. Determination of remotely estimated chl a

Estimates of chl *a* (mg m^{-2}) were based on the relationship between ice algal absorption and ROV-measured spectral transmittance ($T_{(z,\ \lambda)}$) through the snow and sea ice. This relationship was determined with the normalized difference indices (NDI), where

$$\mathrm{NDI} = \left(T_{(z\lambda 1)} - T_{(z\lambda 2)}\right)/\left(T_{(z\lambda 1)} + T_{(z\lambda 2)}\right), \quad (3)$$

for all PAR wavelengths measured by the ROV at the marked locations along the transect (**Figure 1**). These measurements were achieved by manually positioning the ROV next to poles inserted through the ice at known locations (Figure S1), where the colocation accuracy (pole-ROV) was approximately 0.2 m. The success in applying this approach to estimate ice algal chl *a* efficiently has been well-documented (Mundy et al., 2007b; Campbell et al., 2014; Lange et al., 2016). Pearson's correlation surfaces were then constructed between all possible NDI wavelength combinations and ice core-derived chl *a* concentrations to determine the optimal (highest correlation) NDI (Figure S3; 410:423 nm, $r^2 = 0.688$, $P < 0.05$). Following this assessment, chl *a* was calculated using $T_{(z,\ \lambda)}$ and the resultant NDI without physical collection of ice samples, at all ROV measurement locations. For accuracy, ROV data were filtered to remove point locations outside the range of in situ core-based chl *a* that was used to determine the NDI. Finally, we note that transmittance was used in Equation 1 over transmitted irradiance, because it exhibited higher correlation with core-derived chl *a*, as discussed in Mundy et al. (2007b). Chl *a* was also calculated in units of μg L^{-1} for standardization of NCP (described below).

2.3.2. Calculation of hourly and daily production

Hourly estimates of NCP, normalized to chl *a* (μg L^{-1}), were determined by using the in situ estimates of PAR at the ice–water interface ($I_{(ice,\ PAR)}$) in the *P–E* equation for each ice type. PAR at the ice bottom was obtained by correcting the measured PAR at the ROV height ($I_{(ROV,\ PAR)}$) for the additional attenuation of light in the seawater between:

$$I_{(ice,PAR)} = I_{(0,PAR)} \times T_{(ROV,PAR)} \times e^{(D_{ice} \times 0.1)}. \quad (4)$$

Table 2. Average values ± standard deviation for sea ice draft (SID), photosynthetically active radiation (PAR) transmittance (T_{PAR}), daily integrated (24 h) transmitted irradiance of PAR ($I_{(z,\ PAR)}$), chlorophyll *a* (Chl *a*), and net community production (NCP) collected by remotely operated vehicle for a number of point locations (*n*) across spatial grids on May 10, 13, 17, and 22. DOI: https://doi.org/10.1525/elementa.2021.00040.t2

Ice Type	Date (May 2018)	*n*	SID (m)	T_{PAR} (%)	Daily $I_{(z,\ PAR)}$ (mol m^2 d^{-1})	Chl *a* (mg m^{-2})	NCP (μmol O_2 l^{-1} d^{-1})
FYI	10	857	1.14 ± 0.17	0.54 ± 0.26	0.25 ± 0.12	0.89 ± 0.34	−1.10 ± 0.43
	13	61	1.11 ± 0.26	0.50 ± 0.37	0.19 ± 0.14	1.19 ± 0.50	−1.53 ± 0.61
	17	1,112	1.25 ± 0.13	0.62 ± 0.38	0.23 ± 0.14	1.16 ± 0.40	−1.44 ± 0.45
	22	138	1.25 ± 0.42	0.31 ± 0.16	0.15 ± 0.08	0.88 ± 0.40	−1.20 ± 0.55
	All dates	4[a]	1.19 ± 0.24	0.49 ± 0.29	0.21 ± 0.12	1.03 ± 0.41	−1.32 ± 0.51
MYI (All)	10	164	2.29 ± 0.66	0.11 ± 0.08	0.05 ± 0.04	1.07 ± 0.53	−1.24 ± 0.66
	13	92	2.07 ± 0.56	0.13 ± 0.11	0.05 ± 0.04	1.08 ± 0.56	−1.26 ± 0.71
	17	168	2.65 ± 0.73	0.121 ± 0.09	0.05 ± 0.03	1.01 ± 0.53	−1.22 ± 0.70
	22	291	2.43 ± 0.67	0.121 ± 0.09	0.06 ± 0.04	1.02 ± 0.51	−1.16 ± 0.66
	All dates	4	2.36 ± 0.66	0.121 ± 0.09	0.05 ± 0.04	1.04 ± 0.55	−1.22 ± 0.68
MYI_{thick} (>2.4 m)[a]	10	66	2.94 ± 0.34	0.10 ± 0.08	0.04 ± 0.04	1.08 ± 0.51	−1.80 ± 0.77
	13	27	2.74 ± 0.23	0.13 ± 0.12	0.05 ± 0.05	1.08 ± 0.54	−1.80 ± 0.88
	17	113	3.05 ± 0.48	0.11 ± 0.10	0.04 ± 0.04	1.01 ± 0.58	−1.71 ± 0.97
	22	163	2.92 ± 0.33	0.14 ± 0.07	0.07 ± 0.03	0.99 ± 0.54	−1.59 ± 0.91
	All dates	4	2.90 ± 0.35	0.13 ± 0.09	0.05 ± 0.04	1.03 ± 0.54	−1.70 ± 0.88
MYI_{thin} (≤2.4 m)[b]	10	98	1.85 ± 0.34	0.13 ± 0.08	0.06 ± 0.04	1.06 ± 0.51	−1.39 ± 0.77
	13	65	1.79 ± 0.40	0.13 ± 0.12	0.05 ± 0.05	1.08 ± 0.54	−1.48 ± 0.88
	17	55	1.85 ± 0.43	0.14 ± 0.10	0.05 ± 0.04	1.00 ± 0.58	−1.41 ± 0.97
	22	128	1.80 ± 0.41	0.10 ± 0.07	0.07 ± 0.03	1.05 ± 0.54	−1.50 ± 0.91
	All dates	4	1.82 ± 0.40	0.12 ± 0.09	0.05 ± 0.04	1.05 ± 0.54	−1.44 ± 0.88

FYI = first-year sea ice; MYI = multi-year sea ice.

[a]Calculated with May 23 parameters.

[b]Calculated with May 7 parameters.

This approach thus obtains corrected hourly estimates of light in the bottom ice by applying the $T_{(ROV,\ PAR)}$ from a single dive on a given sample day to hourly measurements of surface downwelling irradiance ($I_{(0,\ PAR)}$). A low seawater attenuation coefficient of 0.1 m^{-1} (Fernández-Méndez et al., 2018) in Equation 4 is supported by ROV observations of a visually clear water column throughout the study period. Hourly chl *a*-specific NCP was multiplied by NDI-based chl *a* concentration (μg L^{-1}) and integrated over the 24-h ROV dive date (μmol O_2 d^{-1}). To represent the total light available to the bottom-ice sea ice algae in a given day, we also present the corrected estimate of light availability ($I_{ice,\ PAR}$) over 24 h as $I_{(Z,\ PAR)}$ (mol m^2 d^{-1}).

2.4. Statistical analyses and calculation of spatial grid

Polynomial models of *P–E* curves and the processing of ROV data were completed using Matlab (R2019b) software. Statistical analyses presented were done using SPSS statistical software (IBM Version 20). Comparisons of data between three categories of ice type (FYI, MYI_{Thick}, and MYI_{Thin}) used a one-way analysis of variance (ANOVA) with Fisher's post hoc test, while unpaired *t* test was used for comparison of data between FYI and MYI. Results from these analyses are reported with degrees of freedom (*df*), as well as corresponding *F*-statistic (F_{df}; ANOVA) or *t*-statistic (t_{df}; *t* test). All data were log-transformed prior to analysis if they were not normally distributed by Kolmogorov–Smirnov ($n > 50$) or Shapiro–Wilk test ($n < 50$) or had inhomogeneous variances following a Levene test. Significance of statistical analyses in this research was concluded if $P < 0.05$ for a given test unless otherwise specified. Averages ± standard deviation are presented.

Spatial autocorrelation analyses of ROV-based NCP estimates were performed by fitting an exponential model to empirical semivariograms in Matlab (R2019b) using lag distances binned at 1-m intervals up to a maximum distance of 25 m. Range values of the exponential model, representing patch size of NCP, were determined as the lag

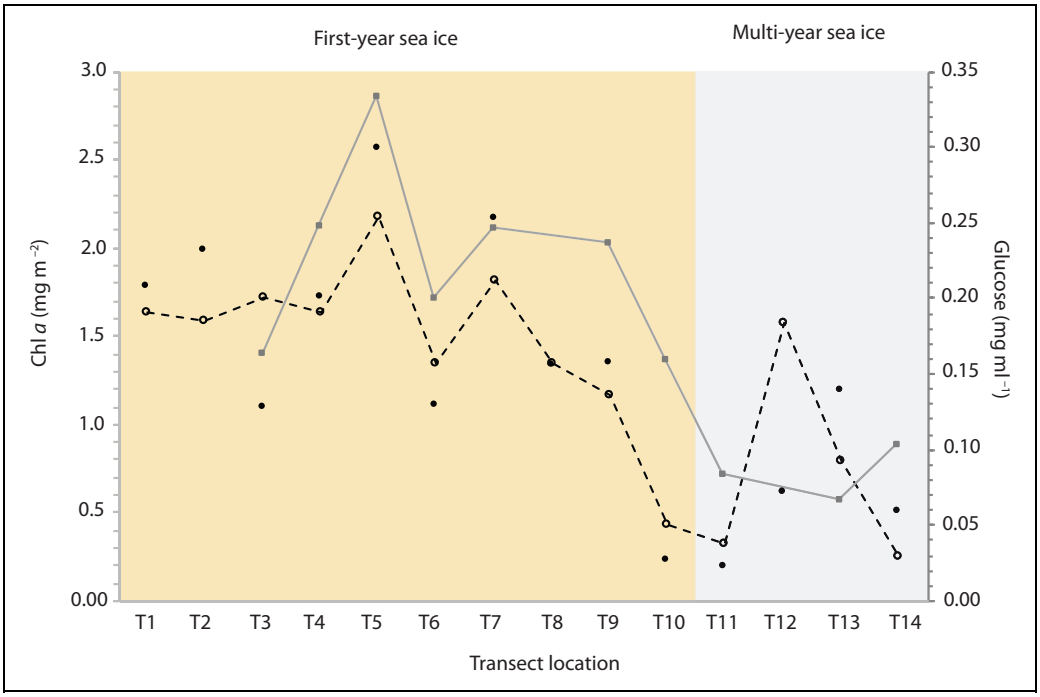

Figure 2. Concentration of chlorophyll *a* (chl *a*) and exopolymeric substances (EPS) across the sampling transect. Chl *a* was measured along the transect either directly from ice cores (solid black circles, no line) or calculated using the normalized difference index (NDI) $NDI_{410:423}$ (hollow black circles, dashed line). The glucose equivalent of EPS in ice cores sampled from sites along the transect is also shown (gray squares, gray line). Yellow shading indicates first-year sea ice; gray shading indicates multi-year sea ice. DOI: https://doi.org/10.1525/elementa.2021.00040.f2

distance at which the model reaches 95% of the sill variance. Goodness of fit (r^2) for each model to sample variance was also calculated. To investigate the impact of irregular patterns of ROV dives on our calculations, ROV-derived measurements (e.g., NCP, chl *a*, $T_{(z,\ PAR)}$) at a given location were linearly interpolated onto a 2-m grid also using the Matlab (R2019b) software. Statistical results presented are for the point-based measurements at an individual ROV-location, unless the use of interpolated gridded data is specified.

3. Results

3.1. Physical site characteristics

The physical characteristics of transect locations on the FYI and MYI floes have been described in detail by Lange et al. (2019), with FYI sites of approximately 140-cm ice thickness and 25-cm snow depth that were consistently thinner than the MYI floe of 300-cm ice and 45-cm snow thickness. All MYI sites on this transect (**Figure 2**), except for T13, had an ice draft of >2.4 m and thus represent MYI_{thick} ice. In comparison to transect locations that were intentionally sampled over a range of snow depths, the additional nontransect ice-core sites for this study targeted comparatively thinner snow covers of about 10–20 cm (**Table 1**), with the exception of relatively thick snow sites on FYI during May 23 sampling (16 cm) and MYI on May 10 (24 cm). Measurements of ice thickness were also higher in the nontransect sites of this study, at approximately 170 cm and 380 cm for FYI and MYI, respectively, compared to the transect mean or values of Lange et al. (2019). Based on ROV measurements of T_{PAR} (**Tables 2** and S2), the average light transmittance available to sea ice algae in the bottom of MYI (0.1 $\pm$ 0.1%) was 5 times lower than in the neighboring FYI floe (0.5 $\pm$ 0.3%).

Between the MYI types, we found that $T_{(Z,\ PAR)}$ and $I_{(Z,\ PAR)}$ of MYI_{thin} and MYI_{thick} were similar (ANOVA post hoc test; for details, see Table S2), with median values around 0.1% and 0.036 mol m^2 d^{-1}. These measurements differed significantly from those of FYI (Table S2), which had a median $T_{(Z,\ PAR)}$ of 0.5% and $I_{(Z,\ PAR)}$ of approximately 0.22 mol m^2 d^{-1} (Table S2). These differences correspond to a greater instantaneous availability of light to algae in FYI than MYI, with average $I_{(ice,\ PAR)}$ of 2.82 $\pm$ 2.06 µmol m^2 s^{-1} under FYI and 0.59 $\pm$ 0.52 µmol m^2 s^{-1} under MYI. Probability density functions for all ROV-based data indicated that the light field (i.e., spatial distribution of light) varied significantly between the respective floes for both point (**Figure 3**) and grid-based (Figure S4) measurements. Here, light transmitted as represented by $T_{(Z,\ PAR)}$ had a broader and more normal distribution for FYI than MYI, while the nearly identical frequency distributions of MYI_{thin} and MYI_{thick} were skewed strongly toward a low light transmittance but with a tail of samples at much higher transmittance.

3.2. Transect measurements of chlorophyll a and EPS

The concentration of chl *a* along the May 23 transect, measured following the collection of ice cores, ranged

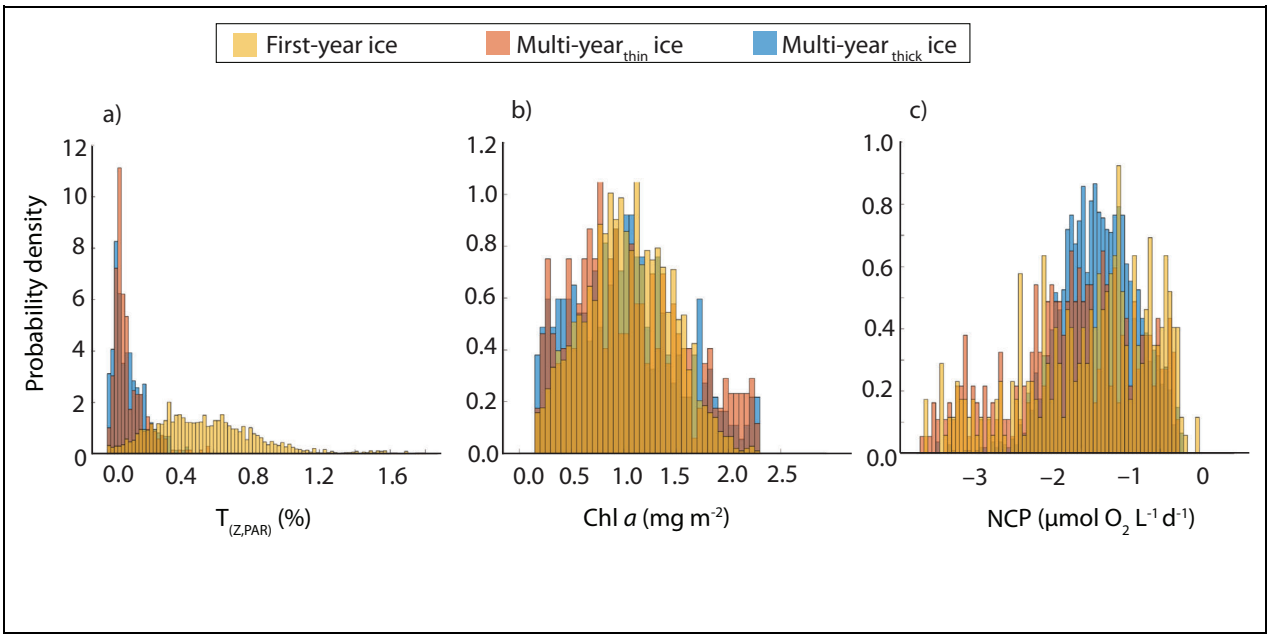

Figure 3. Probability density function of remotely operated underwater vehicle–derived measurements. (a) Transmittance of photosynthetically active radiation ($T_{(z,\ PAR)}$), (b) chlorophyll *a*, and (c) net community production for all point locations sampled across spatial grids of first-year ice (yellow), multi-year thick ice (≥2.4 m; blue), and multi-year thin ice (<2.4 m; red) through the sampling period. Lag distances are binned at a distance of 1 m. DOI: https://doi.org/10.1525/elementa.2021.00040.f3

between 0.23 and 2.56 mg m^{-2} for FYI (mean of 1.53 ± 0.23 mg m^{-2}) and 0.19 and 1.19 mg m^{-2} for MYI (0.62 ± 0.42 mg m^{-2}; **Figure 2**). The chl *a* of MYI cores was highest at the MYI_{thick} location T13. Pearson correlation statistics for all possible NDI wavelength combinations and core-based chl *a* indicated that an NDI based on wavelengths 410 and 423 nm ($NDI_{410:423}$) was the optimal predictor of remotely estimated chl *a* at transect locations, with a coefficient of determination of 0.69 (Figure S3). Remote ROV-based estimates of chl *a* were estimated from the resultant linear regression:

$$\text{chl a}\left(\text{mg m}^{-2}\right) = 23.657\text{mg m}^{-2} \times \text{NDI}_{410:423} + 2.529\text{mg m}^{-2}. \quad (5)$$

The root mean squared error (RMSE) between NDI-derived and core-based chl *a* was 0.39 mg m^{-2} for the entire transect ($n = 14$; **Figure 2**) and was lower for FYI ($n = 10$) versus MYI ($n = 4$) sites with RMSE values of 0.31 and 0.54 mg m^{-2}, respectively. By applying Equation 5 to ROV-based measurements of $T_{(z,\ \lambda)}$, we found that chl *a* was consistently around 1 mg m^2 for the May field season and all ice types, with slightly higher variability in MYI than FYI, as shown by a greater deviation of values around the chl *a* concentration for a given sample day (**Table 2**). Differences in ROV-based chl *a* concentration between ice types were only significant for FYI and MYI_{thick} (Table S2). This difference in chl *a* between FYI and MYI_{thick} of randomized or gridded ROV dives aligns with the significant difference in core-based chl *a* concentration between FYI and MYI across the transect ($t_{12} = 2.541$, $P < 0.05$), which was largely comprised of FYI and MYI_{thick} ice. Normal frequency distributions of chl *a* measured during ROV dives were very similar between FYI, MYI_{thin}, and MYI_{thick} ice (**Figures 3** and S4).

The concentration of EPS in the bottom section of sea ice cores sampled along the transect followed a similar trend to chl *a* (**Figure 2**). This relationship was significant for ice core derived chl *a* ($r^2 = 0.725$, $P < 0.05$) but not for NDI-based chl *a* ($r^2 = 0.431$, $P = 0.055$). The EPS concentrations in FYI (0.237 ± 0.057 mg ml^1) were significantly higher than in MYI (0.109 ± 0.047 mg ml^1; $t_7 = 3.319$, $P < 0.05$).

3.3. Ice algal community composition

Despite similar chl *a* concentrations between ice types (Section 3.2), FYI had consistently higher total cell abundances, although the difference in cell abundance between FYI and MYI was not significant ($t_6 = 0.447$, $P = 0.670$). Nevertheless, the percentage contribution of pennate diatoms within the algal community was significantly greater in FYI ($t_6 = 2.766$, $P < 0.05$; **Figure 4**). In particular, the increase of algal abundance from May 11 to 22 in FYI was attributed to an increasing abundance of the pennate diatom *Pseudonitzschia* spp. The algal community in MYI was also dominated by pennate diatoms and *Pseudonitzschia* spp. However, algal abundance peaked in MYI on May 19 independently of *Pseudonitzschia* spp. abundance, which remained fairly constant throughout the May sampling period. Instead, the peak in algal abundance within MYI was associated with a greater number of centric diatoms in both MYI and FYI on this date and, in particular, a greater abundance of species in the genera of *Attheya* and/or *Chaetoceros*. Overall, MYI harbored higher concentrations of flagellate cells ($t_6 = 1.147$, $P = 0.295$), which accounted for about 40% of the community on May

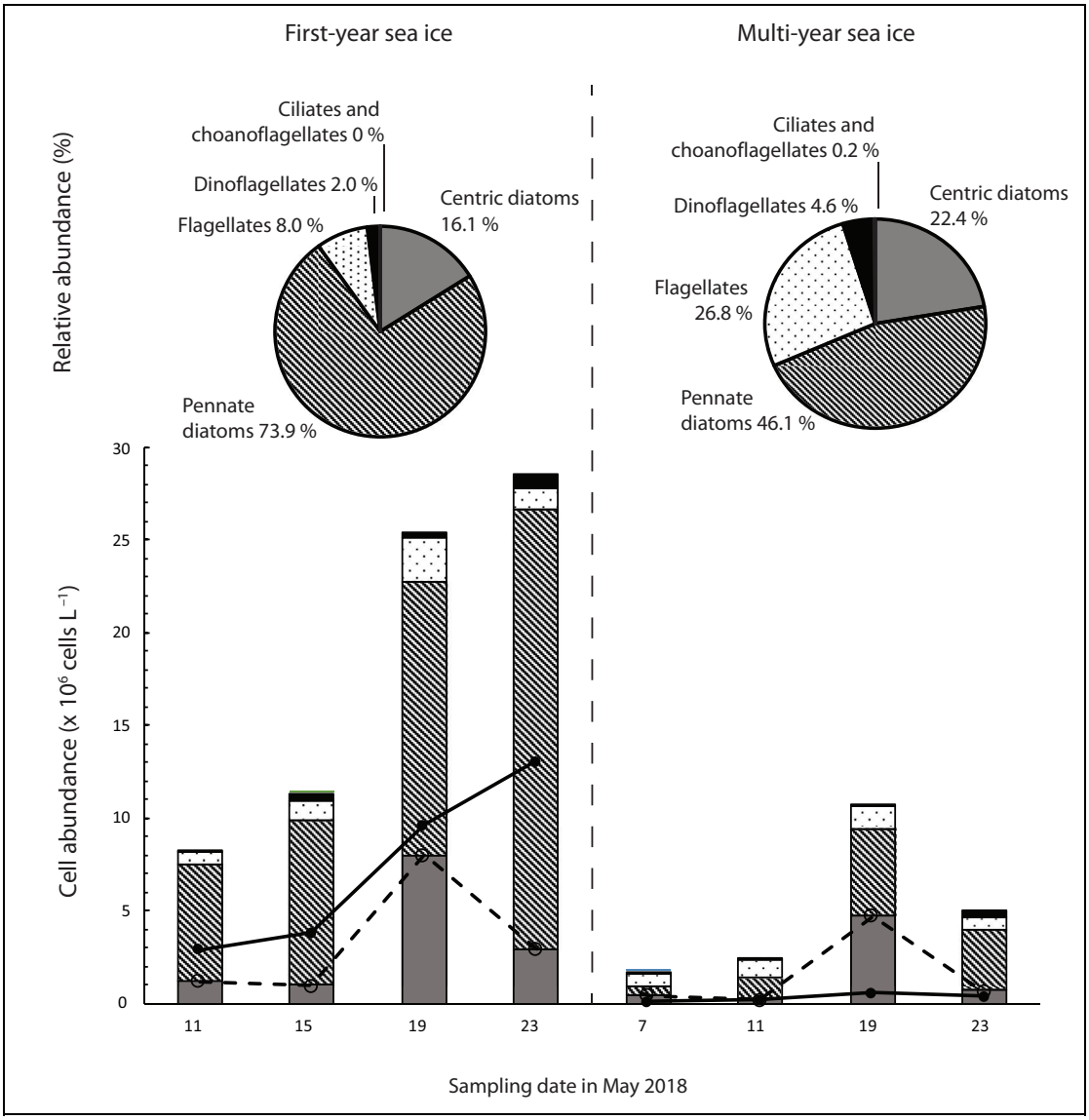

Figure 4. Taxonomic composition of sea ice communities during this study. Average relative (top) and numerical (bottom) abundance of the dominant functional groups observed in samples of first-year sea ice (left) and multi-year sea ice (right) collected through the study period—pennate diatoms (diagonal), centric diatoms (dark gray), and flagellates (dotted), as well as the minor groups of dinoflagellates, ciliates, and choanoflagellates (black). The numerical abundance of the dominant species of pennate diatom *Pseudonitzschia* spp. (solid line) and centric diatom *Attheya/Chaetoceros* spp. (dashed line) are also shown (bottom). DOI: https://doi.org/10.1525/elementa.2021.00040.f4

7 and 11 and 12% later on May 19 and 23. In comparison, flagellate abundance remained below 10% in FYI throughout the spring. Dinoflagellate (<10%), choanoflagellate, and ciliate (<1%) abundances remained low within all ice types and over the entire sampling period.

3.4. Incubation-based photophysiology and nutrient consumption

The *P–E* response of the sea ice algal community in FYI was very similar between early and late spring sampling events (**Table 3**, **Figure 5**). Photoinhibition (b^B) was not observed in either of the two individual FYI production curves. In contrast, *P–E* response differed substantially between the two MYI sampling events, and photoinhibition was observed in both MYI incubations. Within MYI, higher P_m^B, α^B, P_0^B, and I_β, as well as lower b^B, I_k, and I_c, were measured on May 7 MYI_{thin} ice, sampled from non-hummocked ice, versus May 23 MYI_{thick} that represents the *P–E* response of communities within a hummock. Overall, α^B, P_s^B, and P_0^B were lower, and I_k and I_c were higher in FYI than MYI samples. The difference between ice types was significant for the P_s^B parameter ($t_1 = -34.24$, $P < 0.05$).

The concentrations of $NO_3 + NO_2$, PO_4, and $Si(OH_4)$ prior to incubation of FYI on May 23 were 1.44, 0.57, and 1.92 μmol L^{-1}, respectively. Nutrients prior to incubation were largely comparable in MYI on May 7 at 1.13, 0.24, and 1.97 μmol L^{-1} and on May 23 at 1.45, 0.40, and 1.50 μmol L^{-1}, respectively. One exception was PO_4 in MYI on May 7, when the concentration was approximately half in comparison to the other FYI and MYI samples. The

Table 3. Summary of parameters calculated from photosynthesis-irradiance (*P–E*) incubations of first-year (FYI) and multi-year (MYI) sea ice samples, as described by Equation 3. DOI: https://doi.org/10.1525/elementa.2021.00040.t3

Ice Type	Date (May 2018)	$P_s^B(\times 10^{-3})$[a]	$P_m^B(\times 10^{-3})$[b]	$\alpha^B(\times 10^{-4})$[c]	$P_0^B(\times 10^{-3})$[d]	$b^B(\times 10^{-4})$[e]	I_s[f]	I_β[g]	I_c[h]
FYI	4	8.85	—[i]	7.56	6.31	—	11.7	—	14.6
	23	10.5	—	4.21	6.90	—	25.0	—	26.5
	Average of both dates	9.68	—	5.88	6.61	—	18.3	—	20.6
MYI	7 (MYI_{thin})	27.8	16.7	37.2	8.26	0.85	4.48	326	2.66
	23 (MYI_{thick}, hummock)	30.6	8.00	11.4	7.80	3.01	7.03	102	9.04
	Average of both dates	29.2	12.3	24.3	8.13	1.93	5.75	214	5.85

[a]Maximum photosynthetic rate in the absence of photoinhibition (μmol O_2 μg chl a^{-1} h^{-1}).

[b]Maximum photosynthetic rate in the presence of photoinhibition (μmol O_2 μg chl a^{-1} h^{-1}).

[c]Photosynthetic efficiency (μmol O_2 μg chl a^{-1} h^{-1} [μmol photons m^{-2} s^{-1}]$^{-1}$).

[d]Production at zero irradiance (μmol O_2 μg chl a^{-1} h^{-1}).

[e]Slope of photoinhibition portion of *P–E* curve (μmol O_2 μg chl a^{-1} h^{-1} [μmol photons m^{-2} s^{-1}]$^{-1}$).

[f]Photoacclimation parameter (μmol photons m^{-2} s^{-1}).

[g]Index of photoinhibition (μmol photons m^{-2} s^{-1}).

[h]Compensation light intensity (μmol photons m^{-2} s^{-1}).

[i]Emdashes indicate dates when data were not collected.

resultant average ratios of N:P were lower from FYI (2.53) than MYI (4.83, 3.59), while ratios of N: Si were comparable between sample days and ice types (0.75 for FYI, 0.58 and 0.97 for MYI). Nutrient uptake over the May 23 FYI incubation was 4.53×10^{-3} μmol $NO_3 + NO_2$ L^{-1} h^{-1} and 1.12×10^{-3} μmol PO_4 L^{-1} h^{-1}. In MYI, the $NO_3 + NO_2$ uptake was slightly greater and PO_4 lower than FYI, at 4.68×10^{-3} μmol $NO_3 + NO_2$ L^{-1} h^{-1} and 3.58×10^{-4} PO_4 L^{-1} h^{-1} on May 7 and 5.76×10^{-3} μmol $NO_3 + NO_2$ $L^{-1}h^{-1}$ and 3.26×10^{-5} PO_4 L^{-1} h^{-1}, respectively.

3.5. Spatiotemporal variability of first-year ice algal bloom

By applying in situ estimates of PAR irradiance at the ice bottom (Equation 3) into the average *P–E* response function for each ice type (**Figure 5**), daily integrated NCP was shown to be largely negative throughout the study period (**Table 2**) for both ice types. This result indicates consistent net consumption of oxygen by the bottom-ice community and net heterotrophic conditions across the FYI and MYI floes in the month of May. Although there is considerable overlap in the average rates of NCP between the 4 days of ROV operation (**Table 2**), observed differences in NCP between ROV dives were nonetheless significant ($t_{961} = 6.312$, $P < 0.05$). Here, FYI had slightly lower (more negative) NCP than MYI_{avg}, except on May 10.

The grid-based ROV dives on May 10 and 17 under FYI (**Figure 1**) showed similar spatiotemporal dynamics of NCP, including hourly rates of NCP throughout the day and distribution across the ice subsurface (**Figure 6**). We focus on the May 17 grid for further analysis. Areas of greater $T_{(z,\ PAR)}$ produced higher estimates of chl *a* and lower (more negative) rates of NCP. Covariance of NCP over these surfaces, calculated from modeling of semivariograms for point measurements (Figure S6), showed a range (or characteristic algal patch size) of 3.5 m ($r^2 = 0.54$) for May 17. Similarly, this analysis for May 10 (Figure S6) resulted in a patch size of 2.6 m ($r^2 = 0.81$). The hourly changes in NCP over the day were on the order of 0.001 μmol O_2 L^{-1} h^{-1} (**Figure 6**), with diurnal variability producing maximum (least negative) production in late afternoon (5:00 PM on May 10, 4:00 PM on May 17 local time; UTC –4 h) and minimum production (greatest negative) in early morning (4:00 AM on May 10, 3:00 AM on May 17 local time; UTC –4 h). Similar to integrated daily production (**Table 2**), average rates of hourly NCP were consistently greater (less negative) on May 17 versus May 10 in FYI. This difference in average hourly NCP was significant following paired student *t* test ($t_{23} = -38.232$, $P < 0.05$).

4. Discussion

4.1. Contrasting light environments of sea ice habitats

Light available to sea ice algae mainly depends on the thickness and other physical properties of the overlying snow and ice (Stroeve et al., 2021, and references therein). As a result, an inverse relationship between snow and ice thickness and ice algal biomass (e.g., chl *a*, biomass, and cell abundance) has been well-documented prior to the melt season (Mundy et al., 2007a; Campbell et al., 2014, 2015). This inverse relationship may be responsible for the greater accumulation of ice algae in FYI versus MYI across the Arctic (Lange et al., 2015; Lange et al., 2019), except on occasions where dense colonies of the centric diatom *Melosira arctica* have been observed (e.g., Boetius et al., 2013) or where

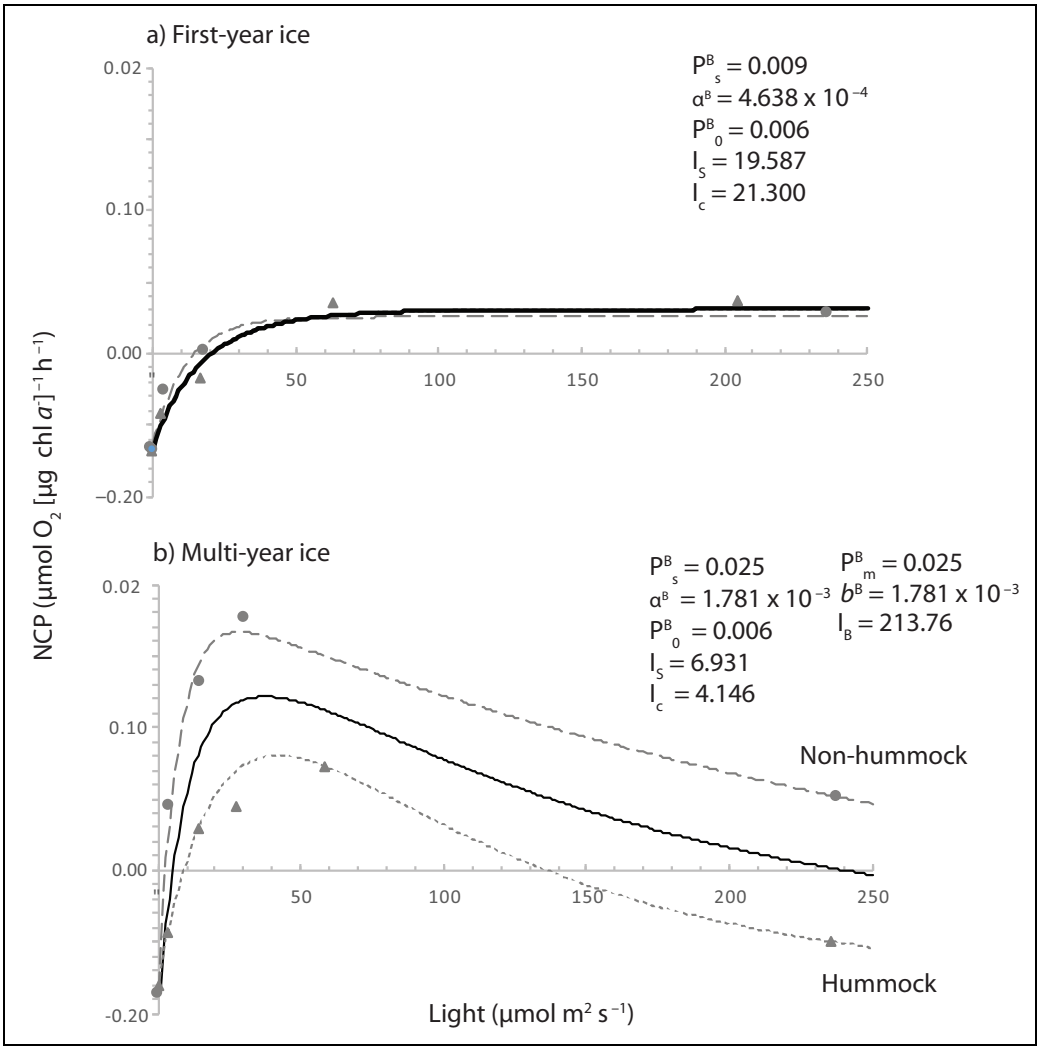

Figure 5. Photosynthesis-irradiance (*P–E*) models of net community production relative to chlorophyll *a*. *P–E* models for (a) first-year sea ice on May 4 (circle) and 23 (triangle) and (b) multi-year sea ice on May 7 (circle) and 23 (triangle). Averaged models (black) and corresponding *P–E* parameters are also shown for each ice type. Definitions of *P–E* parameters are provided in the main text (and in Text S1). DOI: https://doi.org/10.1525/elementa.2021.00040.f5

elevated surfaces (i.e., hummocks) prevent the accumulation of snow (Lange et al., 2017). The significant difference in $T_{(Z,\ PAR)}$ and $I_{(Z,\ PAR)}$ between FYI and MYI habitats in this study (**Table 2**) thus supports the contrasting magnitude of light available to algae within these different ice types. The effect of ice type-dependent light availability on bloom development was not strongly evident in this study, as significant differences in chl *a* were observed only between FYI and MYI_{thick}, which represent the extremes of ice thicknesses sampled.

The impact of variations in MYI thickness on light availability and thus algal growth in MYI is not supported by the results of this study, as we documented similarity in $T_{(Z,\ PAR)}$ and $I_{(Z,\ PAR)}$ between MYI_{thick} and MYI_{thin} despite an average difference in SID of 1.1 m (**Table 2**). We attribute this result to (i) potential differences in snow depth, (ii) limitations in operating the ROV under MYI due to the presence of large ice keels, and/or (iii) an increase in horizontal light scattering with comparatively greater ice thickness of MYI. Unfortunately, we could not measure snow depth across the entire ice surfaces under which the ROV operated, but measurements of snow depth alongside $T_{(Z,\ PAR)}$ across the May 23 transect by Lange et al. (2019) support an inverse relationship between transmittance and snow thickness ($r^2 = 0.59$, $P < 0.05$) that has also been documented in other study regions (Nicolaus et al., 2010; Wang et al., 2014). The deformed subsurface of MYI challenges placement of the ROV platform and thus proximity of light measurements to the bottom-ice interface. Despite this difficulty, the average depth of light measurements beneath FYI and MYI ice–ocean interfaces were both 2.6 m, indicating that the spatial extent of light integrated during a given measurement was similar between the ice types. However, the inherent heterogeneity of MYI (e.g., hummocked and non-hummocked ice) means that a range to sea ice of 2.6 m likely averaged the light intensity measured for comparatively thin and thick MYI despite potentially finer scale variability between these features (Perovich, 1996). The impact of this

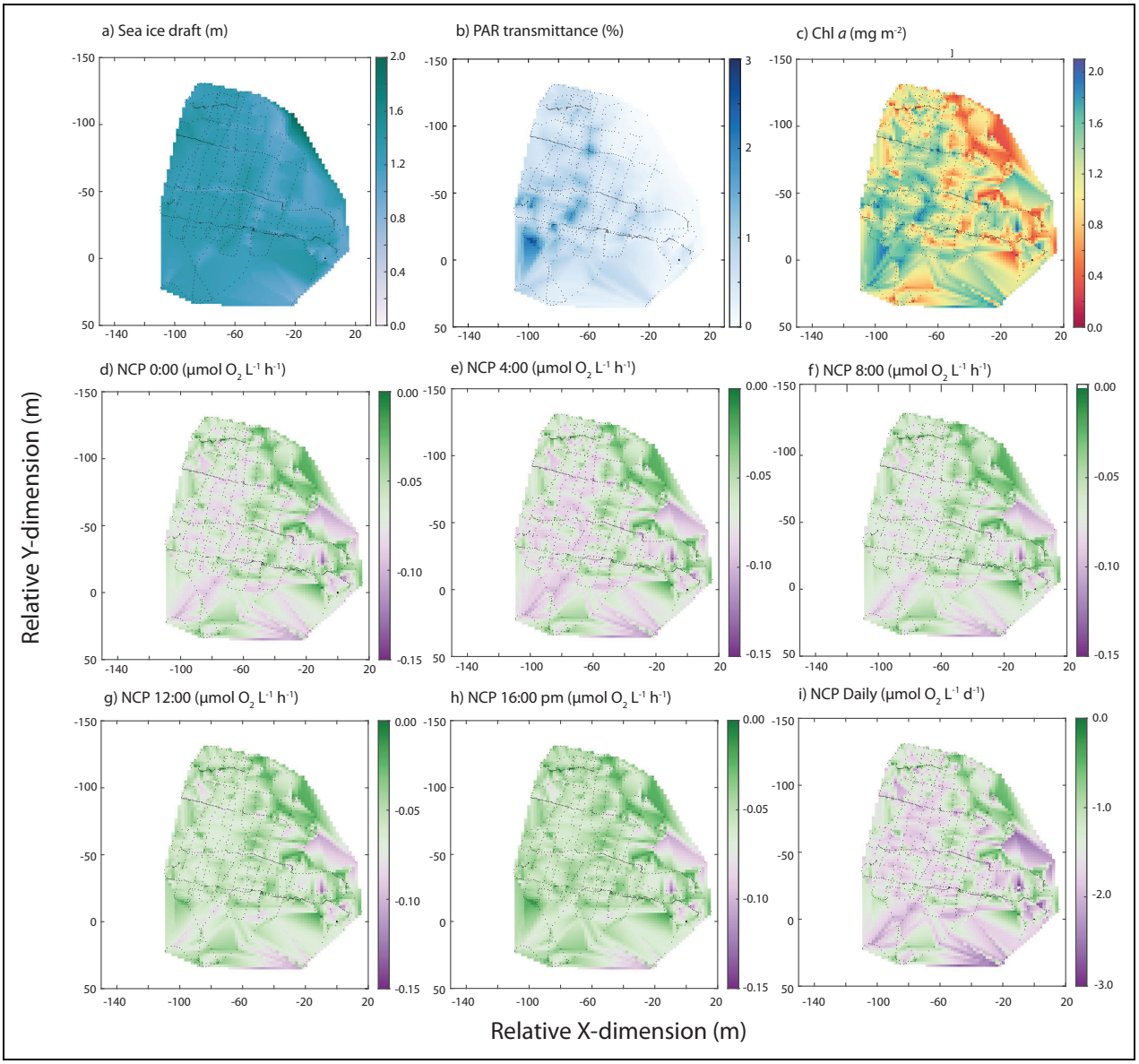

Figure 6. Interpolated surfaces of remotely operated underwater vehicle–based measurements (points) under first-year sea ice on May 17. Included are (a) sea ice draft, (b) transmittance of photosynthetically active radiation, (c) normalized difference indices–derived chlorophyll *a*, and net community production at local hours (d) 12 AM, (e) 4 AM, (f) 8 AM, (g) 12 PM, (h) 4 PM (CET – 4 h), and (i) integrated over 24 h (note the difference in color scale-bar range). DOI: https://doi.org/10.1525/elementa.2021.00040.f6

horizontal scatter is known to increase with ice thickness (Petrich et al., 2012), and thus would have had the greatest influence on MYI measurements.

In addition to differences in the amount of light transmitted through FYI and MYI, we documented a difference in the spatial distribution of light across FYI and MYI floes. Here, FYI was characterized by a light field of greater variability (i.e., greater range of $T_{(Z,\ PAR)}$ measured), while both MYI_{thick} and MYI_{thin} had a smaller range of light values of overall lower intensity (**Figure 3**). Similar to Lange et al. (2019), these differences are thought to be a result of snow drift migration, where the physical presence of drifts is largely uninhibited across level FYI (Iacozza and Barber, 1999) but more limited across a hummocked MYI surface.

4.2. Biogeochemical composition of ice algal communities

Similar to other applications of the NDI method (Mundy et al., 2007b; Campbell et al., 2014; Lange et al., 2016; Wongpan et al., 2018), the optimal NDI wavelengths in this study at 410 and 423 nm overlap with wavelength ranges of maximum chl *a* and minimum ice and snow absorption. The specific NDI wavelengths vary slightly from these studies (e.g., Campbell et al., 2014, report NDI of 478 and 490 nm). Such variability reflects the need to calibrate these indices on a study-by-study basis, so that spatiotemporal differences in algal absorption properties (e.g., pigment composition) or indeed the presence of nonalgal absorbing particulates are accounted for (Mundy et al., 2007b).

Based on the NDI-based calculations, the ROV-derived chl *a* concentrations in this study, around 1 mg m^{-2} (**Figure 2**, **Table 2**), were low in comparison to many other regions of the Arctic (Arrigo et al., 2010). The use of unbuffered melt in this study may have contributed to the measurement of low chl *a* with pigment degradation following low salinity osmotic stress (Campbell et al., 2019). However, these measurements are representative of previous studies on FYI and MYI in the Lincoln Sea (Lange et al., 2015), which also did not practice buffered ice melt. Regardless of these potential impacts on absolute chl *a* concentration and similar to Lange et al. (2015), we found that average chl *a* was slightly higher in MYI than FYI, although overall the chl *a* concentrations were not statistically different between ice types. We hypothesize that similarity in chl *a* between ice types, despite a greater abundance of cells (**Figure 4**) and availability of light in FYI, may have been a combined result of algal light acclimation, widespread nutrient limitation, and potentially the differences in community composition.

Cells in FYI were exposed to light of approximately 0.2 mol m^2 d^{-1} (**Table 2**), equivalent of 2.4 $\pm$ 1.4 μmol m^2 s^{-1}, which is well below the minimum light intensity for photosynthesis (i.e., I_c) at 20 μmol m^2 s^{-1} (**Table 3**). Although the difference between ambient light and I_c indicates clear light limitation, this amount of light in FYI was still greater than that available in MYI at 0.05 mol m^2 d^{-1} (0.6 $\pm$ 0.5 μmol m^2 s^{-1}). The greater light intensities of FYI may have driven a decrease in total chl *a* per cell relative to algae in both MYI_{thick} and MYI_{thin} habitats. Such a photoacclimation response has been documented previously for ice algae (e.g., Michel et al., 1988; Gosselin et el., 1990) and has been hypothesized as the reason for similar chl *a* between snow depths despite differences in cell abundance (Campbell et al., 2018).

The similarity in chl *a* between MYI_{thick} and MYI_{thin} supports previous discussion in this article that the bottom-ice light environment was similar across the MYI habitat due to significant horizontal scattering, which averaged out the influence of smaller scale features like hummocks. It may also indicate similar factors of growth limitation across floes in the region, for example, widespread nutrient limitation in the Lincoln Sea as hypothesized here. For the *P–E* curve samples in this study, ratios of N:P from the start of *P–E* incubations (i.e., T_0 samples) were well below the expected Redfield value of 16 in both FYI and MYI with average values of 2.5 and 4.2, respectively. These low ratios indicate that ice algae in both ice types were potentially experiencing nitrogen-limited growth. Following this rationale, we expect that low nitrogen concentrations account at least in part for the limited accumulation of chl *a* biomass relative to other regions of the Arctic with greater nitrogen availability (Tremblay et al., 2015). Finally, we note that the greater thickness of MYI may increase the habitable space for internal algal communities, which could increase total NDI-derived estimates of chl *a* in MYI relative to FYI. However, higher chl *a* concentrations were found in the mid-ice section in FYI than MYI, indicating that this possibility was not the case (Figure S2).

Our core-based measurements of chl *a* in FYI were somewhat greater than the ROV/NDI-derived estimates, with chl *a* concentration peaking around 2.5 mg m^{-2} along the transect (**Figure 2**). This difference could represent a reduced sensitivity of the NDI method at low biomass (Campbell et al., 2015), which may also explain the insignificant relationship between EPS and NDI-derived chl *a* in this study despite a significant relationship with core-derived chl *a*. Nevertheless, given the strength of the regression (Figure S3), the similarity of ROV-derived chl *a* to previous measurements in the region (Lange et al., 2015), and the limited range of chl *a* in this study (core or ROV-derived), we are confident that the ROV-derived estimates of chl *a* accurately represent biomass across the ice floes.

The relationship between core-based chl *a* and EPS within the bottom ice was more tightly coupled within FYI than MYI (**Figure 2**), as EPS consistently increased with the concentration of chl *a* in FYI. This characteristic positive relationship between chl *a* and EPS is expected considering that the diatoms that dominate sea ice communities represent a major source of EPS, generated for the purposes of cell protection and adhesion to the ice, among other functions (Krembs et al., 2002; Raymond, 2011; Underwood et al., 2013; Aslam et al., 2018). The strength of the relationship within FYI is explained by the relative dominance of pennate diatoms in FYI throughout the study period (**Figure 4**), which are more likely to produce EPS than other functional groups (Underwood and Paterson, 2003). The higher total abundance of EPS-producing cells within FYI was also likely a contributing factor. From a biochemical perspective, sea ice-sourced EPS is a contributor to carbon cycling within marine systems (Riedel et al., 2006; Underwood et al., 2019) and to cloud nucleation in Arctic regions (Kirpes et al., 2019). As a result, our finding that EPS concentration differed between ice types supports that the shift toward a FYI-dominated Arctic along with ongoing climate change (Vihma, 2014; Stroeve et al., 2014) is likely to have consequences for marine and atmospheric chemistry (Underwood et al., 2019). The link to community composition and abundance of pennate species also indicates that potential shifts in sea ice algal community composition, with ongoing environmental change (e.g., Poulin et al., 2011; Hopp et al., 2020), could also have an impact through variability in EPS production.

Previous studies have shown a greater diversity of pennate diatoms in MYI than FYI (Hopp et al., 2020). Instead, the FYI in this study appeared to offer a relatively better habitat for pennate diatom colonization than the MYI (i.e., having a greater relative proportion of pennate diatoms), whereas the MYI offered a relatively better habitat for flagellate colonization than the FYI (i.e., having a greater relative proportion of flagellates). Rather than a difference in species diversity between FYI and MYI, the increasing dominance of pennate diatoms observed within FYI was due to a growing abundance of *Pseudonitzschia* spp. over the spring period, which was not seen in the neighboring MYI. The presence of *Pseudonitzschia* spp. has been documented across the Canadian Arctic (Pućko et al., 2019) and

specifically within sea ice (Różańska et al., 2009). However, this potentially toxic genus is not typically dominant within Arctic sea ice algal blooms (Poulin et al., 2011). The cause of *Pseudonitzschia* spp. growth in this study is difficult to deduce. Provided that nutrient conditions within the region's surface waters and bottom ice (Section 3.4) were relatively homogeneous during the study period, we speculate that the increasing dominance of *Pseudonitzschia* spp. in FYI was a result of the greater acclimation capacity of this genus for high light conditions when compared to other species also present, like *Nitzschia frigida*. Such species-specific preference of sea ice diatoms for seasonally or snow-depth dependent light conditions has been reported previously (Campbell et al., 2018). Although this explanation requires further investigation, it would highlight the increased potential for toxin-producing genera like *Pseudonitzschia* to be competitive in a transition toward sea ice habitats with greater light availability (e.g., thinner ice and snow). Similarly, we note that the greater abundance of flagellate cells in MYI (Comeau et al., 2013) may also be attributed to differences in the physical environment, although the specific driver involved also remains to be explored.

4.3. Algal photophysiology

The similarity of *P–E* response between FYI incubations (**Figure 5**) suggests little spatial or temporal variability in the acclimation state of FYI algae over the spring sampling period, despite a difference in snow cover of approximately 5 cm. In contrast, the photophysiology of MYI algae was considerably different between samples from MYI_{thin} and a visually targeted MYI_{thick} hummock feature, with the hummock having an overlying snow depth that was 20 cm lower (**Table 1**). The thin snow cover characteristic of MYI hummocks has been shown to enhance light transmission to the ice subsurface, despite a greater ice thickness (Lange et al., 2017). As a result, our focused collection of ice cores at the hummock site on May 23 likely sampled algae exposed to greater light intensities than the surrounding non-hummocked ice. We acknowledge the caveat of similarity in $T_{(Z,\ PAR)}$ and $I_{(Z,\ PAR)}$ measured by the ROV for MYI_{thin} and MYI_{thick} (**Table 2**); however, as previously discussed, enhanced horizontal scatter under MYI likely resulted in an integration of the light field beyond the footprint of an individual hummock feature at the measurement depth of the ROV. Due to the combined influence of ice thickness and snow depth, our results imply that light available to bottom-ice algae in this study was likely greatest within FYI and comparable for thick MYI features (e.g., hummocks) and thinner non-hummocked MYI (**Table 2**). This range of light availability is supported by the highest measurements of transmitted light under FYI (**Table 2**) and significant differences in light between only MYI_{thin} and FYI.

The speculated differences in light between sub-habitats contribute to the observed range of photophysiological parameters, where maximum photosynthetic rates in the absence (P_s^B, FYI) or presence of photoinhibition (P_m^B, MYI) and the photosynthetic efficiency (α^B) were lowest in FYI and highest in the non-hummocked MYI on May 4, and I_c and I_k were highest in FYI and lowest in the non-hummock sample (**Table 3**). Photophysiological parameters largely fall within typical ranges of values previously documented for Arctic sea ice algae: P_s^B, 0.007–9.62 mg C [mg chl *a*]$^{-1}$ h^{-1}; α^B, 0.0002–2.15 mg C [mg chl *a*]$^{-1}$ h^{-1} [µmol m^2 s^{-1}]$^{-1}$; I_k, 2–222 µmol m^2 s^{-1} and I_c, 0.18–7.6 µmol m^2 s^{-1}; b^B, 0–2.2 mg C [mg chl *a*]$^{-1}$ h^{-1} [µmol m^2 s^{-1}]$^{-1}$; I_m, 2.7–370 µmol m^2 s^{-1}; I_B, 107–5000 µmol m^2 s^{-1} (Cota, 1985; Gosselin et al., 1985; Bates and Cota, 1986; Irwin, 1990; Johnsen and Hegseth, 1991; Smith and Hermann, 1991). Although, the I_c of FYI algae in this study was particularly high, at the upper end of the range of 0.18–21 µmol m^2 s^{-1} values reported (Cota, 1985; Hsaio, 1988), and I_B measured on the May 23 MYI hummock feature was just below previously documented ranges for FYI.

Although the P_s^B or P_m^B of microalgae often increases as algae adapt to increasing light availability, they may instead display an inverse relationship in instances where photoinhibitory damage is associated with photosystem II of the photosynthetic apparatus (Richardson et al., 1983). A reduced α^B at higher light intensities (e.g., Campbell et al., 2016; Sorrell et al., 2021) may also occur with the influence of photoprotection mechanisms like the production of protective photoprotective pigments, changed size and number of photosynthetic units, as well as modification to the efficiency of electron transport and carboxylating enzymes (Geider and Osborne, 1992). It follows that the algal communities of FYI may have been adapted for high light stress, which would explain the absence of photoinhibition in FYI *P–E* responses (**Figure 5**). That is, the FYI communities did not exhibit photoinhibition because cells were light-adapted against high light intensities, perhaps at an energetic cost to overall growth. Such a photoacclimative state is supported by previous documentation that I_c (Hill 1996) and I_s (Gosselin et al., 1985; Michel et al. 1988; Campbell et al., 2016) of microalgae can increase as ice algae seasonally adapt to increasing light intensity. In contrast to FYI, algae of the lower light MYI habitats we sampled would have been more shade-adapted and thus exhibited a greater sensitivity to high light intensities during incubation, with consistent photoinhibition recorded in the *P–E* responses (**Figure 5**). The differences in photoadaptive state between communities from FYI and MYI in this study suggest that the increasing dominance of FYI in the Arctic (Kwok, 2018) may select for algae with lower photosynthetic potential (P_s^B) but greater resilience to high light intensities (absence of b^B), with uncertain consequences for sea ice NCP.

We note that the robustness or sensitivity of ice algae in this study to highlight intensities was likely coupled to the stability of the light environment. The high mobility of snow across FYI and the resultant high variability in bottom-ice light intensity (**Figure 3**) meant that algae within this habitat could have been exposed periodically to alternating low and high light levels. Such exposure would explain why the average *P–E* response of these algae was fairly consistent over this spring sampling period. Here, potential changes in photophysiology in FYI algae either did not have time to occur with the rate of

drifting snow and thus changing light or they could not be captured by the frequency of incubations in this study. With a dynamic light environment, the overall sensitivity of algae within FYI to light increased experimentally during *P–E* incubations was also limited (i.e., no photoinhibition observed). In contrast, the movement of snow across the deformed MYI surface is more limited (Katlein et al., 2015), which would be consistent with algal communities having a more consistent response under lower light conditions when compared to FYI (**Figure 3**). With subsequent exposure of these shade-adapted communities to highlight intensities during incubation, a high degree of photoinhibition (i.e., high β) would be expected and was observed, especially for the non-hummock sample likely to have been acclimated to the lowest in situ light conditions. In addition, differences in taxonomic composition between FYI and MYI habitats may have contributed to the observed variability in *P–E* response, in particular the abundance of pennate diatom *Pseudonitzschia* spp. in FYI and the greater proportion of flagellates in MYI. We recommend future work to identify the photophysiological characteristics of *Pseudonitzschia* spp. to better understand the role of species-specific responses in sea ice habitats.

4.4. Productivity of FYI and MYI habitats

Despite contrasting light environments, photophysiology, and species composition of sea ice algal communities, the NCP of FYI and MYI was similar, with consistent uptake of O_2 that is indicative of net heterotrophy. Few such O_2-based measurements exist for the Arctic, but these results support previous observations of net heterotrophy in FYI environments by Rysgaard and Glud (2004), Rysgaard et al. (2008), and Campbell et al. (2017), the latter reporting peaks in net O_2 consumption around 3 μmol O_2 l^{-1} h^{-1}. Our results build on these findings by showing the potential for net heterotrophy in MYI habitats in spring, at rates that were higher on average than in FYI. These higher rates may be especially true for MYI hummocks due to greater algal mixotrophy or heterotrophy and/or greater abundance of heterotrophic bacteria. Mixotrophic and heterotrophic species of algae have been documented across ice habitats (Comeau et al., 2013; Søgaard et al., 2021), including species of dinoflagellates that have the potential to increase mixotrophy in the presence of photoinhibitory light intensities (Hee Ok et al., 2019). The visually identified hummock on May 23 had the greatest percentage of dinoflagellates of any sample in this study at 7.3% of total cells enumerated (**Figure 4**). Provided there is higher and more stable light under hummocks as discussed above, MYI_{thick} locations may have had a greater proportion of algae like dinoflagellates that were mixotrophic.

In addition to autotrophic and mixotrophic algae, heterotrophic bacteria, microfauna, and meiofauna likely contributed to the O_2 signals recorded in this study. As bacterial activity was not assessed, we cannot account directly for the influence of heterotrophic bacterial activity versus algal respiration on our O_2-based measurements of production. However, previous studies on bacterial production in sea ice have shown uptake rates that are less than 10% of total NCP (Campbell et al., 2017) and that increase with algal abundance and provision of labile dissolved organic carbon (Mock et al., 1997; Kaartokallio et al., 2013; Campbell et al., 2018). We thus suggest that the O_2 signals of heterotrophy measured here for the Lincoln Sea are likely to be overwhelmingly representative of the ice algal community. Furthermore, the abundance of microfauna like flagellates and ciliates was determined to be low (**Figure 4**), and screening of samples with a 350-μm Nitex screen before incubation would have removed larger meiofauna that could have otherwise influenced measurements over the 36-h incubation period. We also expect that microfauna < 350 μm that potentially persisted within incubation samples had a minimal impact, as previous studies have shown insignificant microzooplankton grazing rates in bottom-ice communities (Michel et al., 2002).

The melting of sea ice samples without addition of FSW has been shown to limit the ^{14}C-based gross primary productivity of sea ice algae (Campbell et al., 2019). While the impact of sample melt procedure on respiration and community productivity remains uncertain, our direct melting approach (i.e., unbuffered) may have also affected our measurements of NCP by enhancing the heterotrophic signal of the incubations. However, such impacts do not affect the comparison of ice types within this study, as the same melt procedure was applied to both samples of FYI and MYI. Furthermore, the average rates of O_2-uptake measured here (**Table 2**) were less than, not greater than, those reported by Campbell et al. (2017) where buffered sample melt was used. Another methodological consideration with the potential to impact the magnitude of O_2 uptake or release reported in this study is the use of transmitted irradiance measured by ROV for calculation of NCP. While these values have been corrected for absorption over depth in the water column (Equation 4), they do not account for the impact of algal absorption or horizontal scatter within the ice (Ehn and Mundy, 2013; Campbell et al., 2017) that could effectively decrease or increase light availability, respectively. Considering the low concentrations of chl *a* in this study and thus the dominating influence of scatter versus absorption, NCP values reported may represent a lower limit of possible production.

The overall relationship between NCP, chl *a*, and $T_{(z,\ PAR)}$ in FYI is evident from representation as spatial grids on May 10 and 17 (**Figures 6** and S5), which is expected given that they are calculated directly from one another. Despite some irregularities as a result of our interpolation method and the distribution of point measurements, the evidence indicates that in the morning between midnight and 8 AM local time, NCP was lower (more negative) in areas of greater chl *a* and $T_{(z,\ PAR)}$, while in the afternoon from 12 to 4 PM, the relationship was largely reversed. This temporal fluctuation corresponds to an enhanced capacity for both heterotrophic (negative NCP) and autotrophic activity (positive NCP) in areas of the ice subsurface where chl *a* biomass was greatest, with the sign of O_2 uptake or release dependent on the magnitude of light available. That is, in the morning, when transmitted irradiance is limited as a result of lower solar angle, the

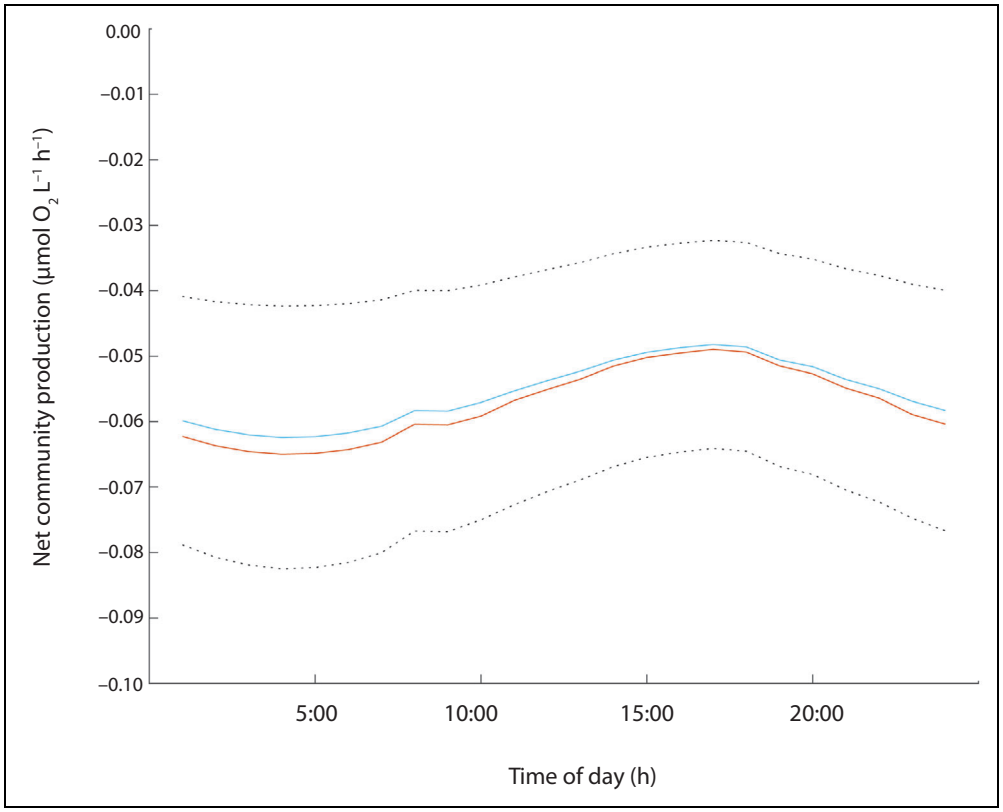

Figure 7. Hourly net community production of first-year sea ice on May 17. Median (orange), mean (blue), and standard deviations (dashed) of remotely operated underwater vehicle–based measurements, with hours marked in local time (GMT−4 h). DOI: https://doi.org/10.1525/elementa.2021.00040.f7

bottom-ice communities had a greater dominance of net heterotrophy compared to times in the afternoon when the angle of downwelling irradiance and thus transmitted PAR was greater. Such variability over the course of a day is an important consideration in the study of sea ice microbial communities, particularly given that a number of primary production or community production estimates for sea ice are provided for a single time point (i.e., hour or day). Instead, the productive state of sea ice varied significantly over the course of the 24-h polar day, which is especially evident when the median and mean (±standard deviation) of hourly NCP is plotted over 24 h (**Figure 7**; see also Figure S7 for May 10). From the overlap or distance between median and mean values, one can also see that the distribution of NCP shifts from approximately Gaussian (normal) during the more light-limited morning (i.e., where the median and mean overlap), to slightly skewed in the afternoon and evening (i.e., where the median and mean deviate). It follows that independently of possible diurnal acclimation (e.g., Mingelbier et al., 1994), in situ production is likely to be more uniform across an ice floe at times of day with lower light intensities that correspond to the initial (and more linear slope) of the *P–E* model. In comparison, times with higher light intensities that approach the transition between the light limited and carbon-fixation steps of photosynthesis (i.e., I_s) may exhibit greater variability between sites. Although further work on diurnal variability of sea ice NCP and primary production is needed, these insights support sample collection in the morning to maximize representativeness of samples for a given ice floe.

This dependence of NCP on light availability is further highlighted by comparing May 10 and 17 surfaces, where the greater NCP (less negative) on May 17 corresponds to a day of slightly greater $T_{(Z,\ PAR)}$ (**Table 2**). In addition to the diurnal variability in FYI production, the 2.6–3.5 m patch size of daily NCP indicates local scale spatial variability across the floe. The size of this patchiness is on the low end of reported values for Arctic and sub-Arctic sea ice with patch sizes ranging from 5 to 90 m (e.g., Gosselin et al., 1986; Rysgaard et al., 2001; Granskog et al., 2005; Søgaard et al., 2010; Wongpan et al., 2020) and is likely the result of the distribution of snow cover. This complex relationship between the spatial variability of ice algal chl *a* and production with physical-biogeochemical drivers remains a poorly constrained aspect of sea ice algal phenological studies.

5. Conclusion

In this study, we have shown widespread heterotrophy (O_2 uptake) across FYI and MYI floes during the High Arctic spring, despite significantly greater transmission of light through the younger ice cover. The differing light conditions determined by spatiotemporal ice thickness and snow depth affected the photophysiology of algal communities living within the bottom ice and were possibly the cause of differences in species composition. The algal communities of FYI were acclimated for comparatively high

light conditions compared to MYI, with mechanisms of photoprotection potentially limiting their photosynthetic potential during the spring sampling period. In contrast, the ice algal community within two classes of MYI thickness was consistently shade-acclimated and showed high photoinhibition during *P–E* incubations. These differences highlight that in a changing icescape, a younger ice cover with greater light availability and variability may not necessarily result in a more productive system. That is, considering the NCP of sea ice habitats, an increasing dominance of FYI may not result in a stronger autotrophic signal (O_2 release and CO_2 uptake) from the bottom sea ice habitats. Instead, further considerations are critical for accurate projection of sea ice biogeochemistry in a changing climate, including the energetic costs of respiration, photoprotection, and mixotrophy, as well as the presence of flagellates and genera like toxin-producing *Pseudonitzschia*.

The overall similarity of NCP between FYI and MYI floes of the Lincoln Sea (**Table 2**) was in contrast to the variability in chl *a* at the local 2.6–3.5 m scale of algal patchiness under FYI and to the substantial variability in topography across the hummocked MYI surface. Like the known influence of snow on algal acclimation state, these smaller scale subfloe differences in light resulting from dynamics of the overlying snow cover appeared to drive variability that would have otherwise been lost from a larger scale perspective. Combined with this insight, we have documented diurnal variability of NCP in FYI, which varies with downwelling irradiance and influences the productive state (i.e., autotrophic or heterotrophic) of the ice. From this work, we stress the importance of future sea ice research that combines sampling over multiple spatiotemporal scales and further develops methodologies that permit remote study of algal blooms across them. From such developments, ice-floe-scale biomass and productivity of sea ice algal blooms may be represented more accurately. Potential modeling efforts, supported by observational data, may help to determine the impact of changing snow and ice cover on marine ecosystem function and biogeochemistry.

Data accessibility statement

Remotely operated underwater vehicle data are available on Pangea (10.1594/PANGEA.901247). Biogeochemical data sets are available in the Polar Data Catalogue (NE/R012849/1).

Supplemental files

The supplemental files for this article can be found as follows:

This research includes supplementary material (Text S1 List of abbreviations, Tables S1 and S2, Figures S1–S7) that has been uploaded separately to this document.

Acknowledgment

Special thank you to Andrew Platt (Environment Canada), Arttu Jutila, Jana Hildebrand, and Ron ten Boer (AWI) for their assistance during the Lincoln Sea field campaign.

Funding

This work is a contribution to the Diatom ARCTIC project (NE/R012849/1; 03F0810A), part of the Changing Arctic Ocean program, jointly funded by the UKRI Natural Environment Research Council and the German Federal Ministry of Education (BMBF), and the Fisheries and Oceans Canada (DFO) Science and the Marine Productivity Laboratory Program. The Multidisciplinary Arctic Program—Last Ice is funded by Fisheries and Oceans Canada (DFO) Science in support of Tuvaijuittuq Marine Protected Area. Additional support was provided by Polar Continental Shelf Program (Project 10718) and the Natural Sciences and Engineering Research Council of Canada Discovery Funds to CM and CHSR. The AWI remotely operated underwater vehicle work was funded by the Helmholtz strategic investment Frontiers in Arctic Marine Monitoring. JL was supported in part by the Centre for Integrated Remote Sensing and Forecasting for Arctic Operations funded by the Research Council of Norway (project number 237906).

Competing interests

Authors have no competing interests to declare. CM is an associate editor in the Ocean Science knowledge domain. She was not involved in the review process of this article.

Author contributions

Concept and design: KC, JCL, BAL, CK.

Acquisition, analysis, and interpretation of data: KC, BAL, CK, PA, JC, SD, PT, CM.

Drafting and revising of this article, approval for publication: All authors.

References

Arrigo, KR, Mills, MM, Kropuenske, LR, van Dijken, GL, Alderkamp, AC, Robinson, DH. 2010. Photophysiology in two major Southern Ocean phytoplankton taxa: Photosynthesis and growth of *Phaeocystis antarctica* and *Fragilariopsis cylindrus* under different irradiance levels. *Integrative and Comparative Biology* **50**: 950–966. DOI: http://dx.doi.org/10.1093/icb/icq021.

Aslam, SN, Strauss, J, Thomas, DN, Mock, T, Underwood, GJC. 2018. Identifying metabolic pathways for production of extracellular polymeric substances by the diatom *Fragilariopsis cylindrus* inhabiting sea ice. *The ISME Journal* **12**: 123–125. DOI: http://dx.doi.org/10.1038/s41396-017-0039-z.

Bates, SS, Cota, GF. 1986. Fluorescence induction and photosynthetic responses of Arctic ice algae to sample treatment and salinity. *Journal of Phycology* **22**: 421–429.

Boetius, A, Albrecht, S, Bakker, K, Bienhold, C, Felden, J, Fernández-Méndez, M, Hendricks, S, Katlein, C, Lalande, C, Krimpen, T, Nicolaus, M, Peeken, I, Rabe, B, Rogacheva, A, Rybakpva, E, Somavilla, R, Wenzhöfer, F, RV Polarstern ARK27-3-Shipboard Science Party. 2013. Export of algal biomass from the melting Arctic sea ice. *Science* **339**(6126):

1430–1432. DOI: http://dx.doi.org/10.1126/science.1231346.

Campbell, K, Mundy, CJ, Barber, DG, Gosselin, M. 2014. Remote estimates of ice algae biomass and their response to environmental conditions during spring melt. *Arctic* **67**(3): 375–387. DOI: http://dx.doi.org/10.14430/arctic4409.

Campbell, K, Mundy, CJ, Barber, DG, Gosselin, M. 2015. Characterizing the sea ice algae chl a-snow depth relationship over Arctic spring melt using transmitted irradiance. *Journal of Marine Systems* **127**: 76–84. DOI: http://dx.doi.org/10.1016/j.jmarsys.2014.01.008.

Campbell, K, Mundy, CJ, Belzile, C, Delaforge, A, Rysgaard, S. 2018. Seasonal dynamics of algal and bacterial communities in Arctic sea ice under variable snow cover. *Polar Biology* **41**(1): 41–58. DOI: http://dx.doi.org/10.1007/s00300-017-2168-2.

Campbell, K, Mundy, CJ, Gosselin, M, Landy, JC, Delaforge, A, Rysgaard S. 2017. Net community production in the bottom of first-year sea ice over the Arctic spring bloom. *Geophysical Research Letters* **44**: 8971–8978. DOI: http://dx.doi.org/10.1002/2017GL074602.

Campbell, K, Mundy, CJ, Juhl, AR, Dalman, LA, Michel, C, Galley, RJ, Else, BE, Geilfus, NX, Rysgaard, S. 2019. Melt procedure affects the photosynthetic response of sea ice algae. *Frontiers in Earth Sciences* **7**(21): 1–14. DOI: http://dx.doi.org/10.3389/feart.2019.00021.

Campbell, K, Mundy, CJ, Landy, JC, Delaforge, A, Michel, C, Rysgaard, S. 2016. Community dynamics of bottom-ice algae in Dease Strait of the Canadian Arctic. *Progress in Oceanography* **149**: 27–19. DOI: http://dx.doi.org/10.1016/j.pocean.2016.10.005.

Castellani, G, Schaafsma, FL, Arndt, S, Lange, B, Peeken, I, Ehrlich, E, David, C, Ricker, R, Krumpen, T, Hendricks, S, Schwegmann, S, Massicotte, P, Hlores, H. 2020. Large-scale variability of physical and biological sea-ice properties in polar oceans. *Frontiers in Marine Science*: **7**(536): 1–22. DOI: http://dx.doi.org/10.3389/fmars.2020.00536.

Cimoli, E, Meiners, K, Lund-Hansen, L, Lucieer, V. 2017. Spatial variability in sea-ice algal biomass: An under-ice remote sensing perspective. *Advances in Polar Science* **28**(4): 268–296. DOI: http://dx.doi.org/10.13679/j.advps.2017.4.00268.

Comeau, AM, Philippe, B, Thaler, M, Gosselin, M, Poulin, M, Lovejoy, C. 2013. Protists in Arctic drift and land-fast sea ice. *Journal of Phycology* **49**: 229–240. DOI: http://dx.doi.org/10.1111/jpy.12026.

Cota, G, Smith REH. 1991. Ecology of bottom ice algae: II, Dynamics, distributions and productivity. *Journal of Marine Systems* **2**: 279–295. DOI: http://dx.doi.org/10.1016/0924-7963(91)90037-U.

Cota, GF. 1985. Photoadaptation of high Arctic ice algae. *Nature* **315**: 219–221.

Dubois, M, Gilles, KA, Hamilton, JK, Rebers, PA, Smith F. 1956. Colorimetric method for determination of sugars and related substances. *Analytical Chemistry* **28**(3): 350–356.

Ehn, JK, Mundy, CJ. 2013. Assessment of light absorption within highly scattering bottom sea ice from under-ice light measurements: Implications for Arctic ice algae primary production. *Limnology and Oceanography* **58**(3): 893–902. DOI: http://dx.doi.org/10.4319/lo.2013.58.3.0893.

Fernández-Méndez, M, Katlein, C, Rabe, B, Nicolaus, M, Peeken, I, Bakker, K, Flores, H, Boetius, A. 2015. Photosynthetic production in the central Arctic Ocean during the record sea-ice minimum in 2012. *Biogeosci*ences **12**: 3525–3549. DOI: http://dx.doi.org/10.5194/bg-12-3525-2015.

Fernández-Méndez, M, Olsen, LM, Kauko, HM, Meyer, A, Rosel, A, Merkouriadi, I, Mundy, CJ, Ehn, JK, Johansson, AM, Wagner, PM, Ervik, A, Sorrell, BK, Duarte, P, Wold, A, Hop, H, Assmy P. 2018. Algal hot spots in a changing Arctic Ocean: Sea-ice ridges and the snow-ice interface. *Frontiers in Marine Science* **5**(75). DOI: http://dx.doi.org/10.3389/fmars.2018.00075.

Fortier, M, Fortier, L, Michel, C, Legendre, L. 2002. Climatic and biological forcing of the vertical flux of biogenic particles under seasonal arctic sea ice. *Marine Ecology Progress Series* **225**: 1–16. DOI: http://dx.doi.org/10.3354/meps225001.

Geider, RJ, Osborne, BA. 1992. *Algal photosynthesis: The measurements of algal gas exchange, current phycology 2*. Boston, MA: Springer Science.

Gosselin, M, Legendre, L, Demers, S, Ingram, RG. 1985. Responses of sea-ice microalgae to climatic and fortnightly tidal energy inputs (Manitounuk Sound, Hudson Bay). *Canadian Journal of Fisheries and Aquatic Sciences* **42**: 999–1006. DOI: http://dx.doi.org/10.1139/f85-125.

Gosselin, M, Legendre, L, Therriault, J-C, Demers, S. 1990. Light and nutrient limitation of sea-ice microalgae (Hudson Bay, Canadian Arctic). *Journal of Phycology* **26**: 220–232. DOI: http://dx.doi.org/10.1111/j.0022-3646.1990.00220.x.

Gosselin, M, Legendre, L, Therriault, JC, Demers, S, Rochet, M. 1986. Physical control of the horizontal patchiness of sea-ice microalgae. *Marine Ecology Progress Series* **29**: 289–298. DOI: http://dx.doi.org/10.3354/meps029289.

Gosselin, M, Levasseur, M, Wheeler, PA, Horner, RA, Booth, BC. 1997. New measurements of phytoplankton and ice algal production in the Arctic Ocean. *Deep-Sea Res*earch *II* **44**(8): 1623–1644. DOI: http://dx.doi.org/10.1016/S0967-0645(97)00054-4.

Gradinger, R. 1999. Vertical fine structure of algal biomass and composition in Arctic pack ice. *Marine Biology* **133**: 745–754. DOI: http://dx.doi.org/10.1139/f90-154.

Granskog, MA, Kaartokallio, H, Kuosa, H, Thomas, DN, Ehn, J, Sonninen, E. 2005. Scales of horizontal patchiness in chlorophyll a, chemical and physical properties of landfast sea ice in the Gulf of Finland

(Baltic Sea). *Polar Biology* **28**: 276–283. DOI: http://dx.doi.org/10.1007/s00300-0040690-5.

Grenfell, TC, Maykut, GA. 1977. The optical properties of ice and snow in the Arctic basin. *Journal of Glaciology* 18(80): 445–463. DOI: http://dx.doi.org/10.3189/S0022143000021122.

Hee Ok, JH, Jeong, HJ, Lim, AN, You, JH, Kang, HC, Kim, SJ, Lee, SY. 2019. Effects of light and temperature on the growth of *Takayama helix* (Dinophyceae): Mixotrophy as a survival strategy against photoinhibition. *Journal of Phycology* **55**(5): 1181–1195. DOI: http://dx.doi.org/10.1111/jpy.12907.

Hill, W. 1996. *Effects of light in algal ecology freshwater benthic ecosystems*. Academic Press. DOI: http://dx.doi.org/10.1016/B978-012668450-6/50034-5.

Hopp H, Vihtakari, M, Bluhm, BA, Assmy, P, Poulin, M, Gradinger, R, Peeken, I, Quillfeldt, C, Olsen, LM, Zhitina, L, Melnikov, IA. 2020. Changes in sea-ice protist diversity with declining sea ice in the Arctic Ocean from the 1980s to 2010s. *Frontiers in Marine Science* **7**(243): 1–18. DOI: http://dx.doi.org/10.3389/fmars.2020.00243.

Hsaio, SIC. 1988. Spatial and seasonal variations in primary production of sea ice microalgae and phytoplankton in Frobisher Bay, Arctic Canada. *Marine Ecology Progress Series* **44**: 275–285.

Iacozza, J, Barber, D. 1999. An examination of the distribution of snow on sea-ice. *Atmosphere- Ocean* **1**: 21–51. DOI: http://dx.doi.org/10.1080/07055900.1999.9649620.

Irwin, BD. 1990. Primary production of ice algae on a seasonally-ice-covered, continental shelf. *Polar Biology* **10**: 247–254.

Johnsen, G, Hegseth, EN. 1991. Photoadaptation of sea-ice microalgae in the Barents Sea. *Polar Biology* **11**: 179–184.

Kaartokallio, H, Søgaard, DH, Norman, L, Rysgaard, S, Tison, JL, Delille, B, Thomas, DN, 2013. Short-term variability in bacterial abundance, cell properties, and incorporation of leucine and thymidine in subarctic sea ice. *Aquatic Microbial Ecology* **71**: 57–73. DOI: http://dx.doi.org/10.3354/ame01667.

Katlein, C, Arndt, S, Belter, HJ, Castellani, G, Nicolaus, M. 2019. Seasonal evolution of light transmission distributions through Arctic sea ice. *Journal of Geophysical Research: Oceans* **24**: 5418–5435. DOI: http://dx.doi.org/10.1029/2018jc014833.

Katlein, C, Arndt, S, Nicolaus, M, Perovich, DK, Jakuba, MV, Suman, S, Elliott, S, Whitcomb, LL, McFarland, CJ, Gerdes, R, Boetius, A, CR German. 2015. Influence of ice thickness and surface properties on light transmission through Arctic sea ice. *Journal of Geophysical Research: Oceans* **120**(9): 5932–5944. DOI: http://dx.doi.org/10.1002/2015JC010914.

Katlein, C, Schiller, M, Belter, HJ, Coppolaro, V, Wenslandt, D, Nicolaus, M. 2017. A new remotely operated sensor platform for interdisciplinary observations under sea ice. *Frontiers in Marine Science* **4**(281): 1–12. DOI: http://dx.doi.org/10.3389/fmars.2017.00281.

Kennedy, F, Martin, A, Castrisios, K, Cimoli, E, McMinn, A, Ryan, KG. 2020. Rapid manipulation in irradiance induces oxidative free-radical release in a fast-ice algal community (McMurdo Sound, Antarctica). *Frontiers in Plant Sciences* **11**: 588005. DOI: http://dx.doi.org/10.3389/fpls.2020.588005.

Kirpes, RM, Bonanno, D, May, NW, Fraund, M, Barget, AJ, Moffet, RC, Ault, AP, Pratt KA. 2019. Wintertime Arctic sea spray aerosol composition controlled by sea ice lead microbiology. *ACS Central Science* **5**(11): 1760–1767. DOI: http://dx.doi.org/10.1021/acscentsci.9b00541.

Krembs, C, Deming, JW, Junge, K, Eicken, H. 2002. High concentrations of exopolymeric substances in wintertime sea ice: Implications for the polar ocean carbon cycle and cryoprotection of diatoms. *Deep-Sea Research I* **49**: 2163–2181. DOI: http://dx.doi.org/10.1016/S0967-0637(02)00122-X

Kwok, R. 2018. Arctic sea ice thickness, volume, and multiyear ice coverage: losses and coupled variability (1958–2018). *Environmental Research Letters* **13**(10): 105005. DOI: http://dx.doi.org/10.1088/1748-9326/aae3ec

Lange, BA, Flores H, Michel C, Beckers JF, Bublitz A, Casey JA, Castellani, G, Hatam, I, Reppchen, A, Rudolph, SA, Haas, C. 2017. Pan-Arctic sea ice-algal chl *a* biomass and suitable habitat are largely underestimated for multi-year ice. *Global Change Biology* **23**(11): 4581–4597. DOI: http://dx.doi.org/10.1111/gcb.13742.

Lange, BA, Haas, C, Charette, J, Katlein, C, Campbell, K, Duerksen, S, Coupel, P, Anhaus, P, Jutila, A, Tremblay, POG, Carlyle, C, Michel, C. 2019. Contrasting ice algae and snow-dependent irradiance relationships between first-year and multiyear sea ice. *Geophysical Research Letters* **46**: 10834–10843. DOI: http://dx.doi.org/10.1029/2019GL082873.

Lange, BA, Katlein, C, Nicolaus, M, Peeken, I, Flores, H. 2016. Sea ice algae chlorophyll *a* concentrations derived from under-ice spectral radiation profiling platforms. *Journal of Geophysical Research: Oceans* **121**: 8511–8534. DOI: http://dx.doi.org/10.1002/2016JC011991.

Lange, BA, Michel, C, Beckers, JF, Casey, JA, Flores, H, Hatam, I, Meisterhans, G, Niemi, A, Haas, C. 2015. Comparing springtime ice-algal chlorophyll a and physical properties of multi-year and first-year sea ice from the Lincoln Sea. *PLoS One* **10**(4): e0122418. DOI: http://dx.doi.org/10.1371/journal.pone.0122418.

Lannuzel, D, Tedesco, L, van Leeuwe, M, Campbell, K, Flores, H, Delille, B, Miller, L, Stefels, J, Assmy, P, Bowman, J, Brown, K, Castellani, G, Chierici, M, Crabeck, O, Damm, E, Else, B, Fransson, A, Fripiat, F, Geilfus, N-X, Jacques, C, Jones, E, Kaartokallio, H, Kotovitch, M, Meiners, K, Moreau, S, Nomura, D, Peeken, I, Rintala, J-M, Steiner, N,

Tison, J-L, Vancoppenolle, M, der Linden, FV, Vichi, M, Wongpan, P. 2020. The future of Arctic sea-ice biogeochemistry and ice-associated ecosystems. *Nature Climate Change* **10:** 983–992. DOI: http://dx.doi.org/10.1038/s41558-020-00940-4.

Leu, E, Mundy, CJ, Assmy, P, Campbell, K, Gabrielsen, TM, Gosselin, M, Juul-Pedersen, T, Gradinger, R. 2015. Arctic spring awakening—Steering principles behind the phenology of vernal ice algae blooms. *Progress in Oceanography* **139**: 151–170. DOI: http://dx.doi.org/10.1016/j.pocean.2015.07.012.

Maslanik, JA, Fowler, C, Stroeve, J, Drobot, S, Zwally, J, Yi, D, Emery, W. 2007. A younger, thinner Arctic ice cover: Increased potential for rapid, extensive ice sea-ice loss. *Geophysical Research Letters* **34**(L24501). DOI: http://dx.doi.org/10.1029/2007GL032043.

Matthes, L, Mundy, CJ, Girard, SL, Babin, M, Verin, G, Ehn, JK. 2020. Spatial heterogenerity as a key variable influencing spring-summer progression in UVR and PAR transmission through Arctic sea ice. *Frontiers in Marine Science* **7**(183). DOI: http://dx.doi.org/10.3389/fmars.2020.00183.

Michel, C, Legendre, L, Demers, S, Therriault, J-C. 1988. Photoadaptation of sea-ice microalgae in springtime: Photosynthesis and carboxylating enzymes. *Marine Ecology Progress Series* **50**: 177–185. DOI: http://dx.doi.org/10.3354/meps050177.

Michel, C, Legendre, L, Ingram, RG, Gosselin, M, Levasseur, M. 1996. Carbon budget of ice algae under first-year ice: Evidence of a significant transfer to zooplankton grazers. *Journal of Geophysical Research* **101**(C8): 18345–18360. DOI: http://dx.doi.org/10.1029/96JC00045.

Michel, C, Nielsen, TG, Gosselin, M, Nozais, C. 2002. Significance of sedimentation and grazing by ice micro- and meiofauna for carbon cycling in annual sea ice (Northern Baffin Bay). *Aquatic Microbial Ecology* **30**: 57–68. DOI: http://dx.doi.org/10.3354/ame030057.

Mingelbier, M, Klein, B, Claereboudt, MR, Legendre, L. 1994. Measurement of daily primary production using 24 h incubations with the ^{14}C method: a caveat. *Marine Ecology Progress Series* **113**: 301–109. DOI: http://dx.doi.org/10.33 http://doi.org/54/MEPS11301.

Mock, T, Meiners, KM, Giesenhagen, HC. 1997. Bacteria in sea ice and underlying brackish water at 54" 26' 50'' N (Baltic Sea, Kiel Bight). *Marine Ecology Progress Series* **158**: 23–40. DOI: http://dx.doi.org/10.3354/meps158023.

Moreau, S, Vancoppenolle, M, Bopp, L, Aumont, O, Madec, G, Delille, B, Tison, J-L, Barriat, P-Y, Goosse, H. 2016. Assessment of the sea-ice carbon pump: Insights from a three-dimensional ocean-sea-ice biogeochemical model (NEMI-LIM-PISCES). *Elementa Science of the Anthropocene* **4**: 00012. DOI: http://dx.doi.org/10.12952/journal.elementa.000122.

Mundy, CJ, Barber, DG, Michel, C, Marsden, RF. 2007a. Linking ice structure and microscale variability of algal biomass in Arctic first-year sea ice using an in situ photographic technique. *Polar Biol*ogy **30**: 1099–1114. DOI: http://dx.doi.org/10.1007/s00300-007-0267-1.

Mundy, CJ, Ehn, JK, Barber, DG, Michel, C. 2007b. Influence of snow cover and algae on the spectral dependence of transmitted irradiance through Arctic landfast first-year sea ice. *Journal of Geophysical Research* **112**: C03007. DOI: http://dx.doi.org/10.1029/2006JC003683.

Nicolaus, M, Gerland, S, Hudson, SR, Hanson, S, Haapala, J, Perovich, DK. 2010. Seasonality of spectral albedo and transmittance as observed in the Arctic Transpolar Drift in 2007. *Journal of Geophysical Research* **115**(C11011). DOI: http://dx.doi.org/10.1029/2009JC006074.

Nicolaus, M, Katlein, C, Maslanik, J, Hendricks, S. 2012. Changes in Arctic sea ice result in increasing light transmittance and absorption. *Geophysical Research Letters* **39**(24): L24501. DOI: http://dx.doi.org/10.1029/2012GL053738.

Nicolaus, M, Petrich, C, Hudson, SR, Granskog, MA. 2013. Variability of light transmission through Arctic land-fast sea ice during spring. *The Cryosphere* **7**: 977–986. DOI: http://dx.doi.org/10.5194/tc-7-977-2013.

Parsons, TR, Maita, Y, Lalli, CM. 1984. *Manual of chemical and biological methods for seawater analysis*. New York, NY: Pergamon Press.

Perovich, DK. 1990. Theoretical estimates of light reflection and transmission by spatially complex and temporally varying sea ice covers. *Journal of Geophysical Research* 95(C6): 9557– 9567. DOI: http://dx.doi.org/10.1029/JC095iC06p09557.

Perovich, DK. 1996. *The optical properties of sea ice*. Springfield, VA: US Army Corps of Engineers: 1–25.

Petrich, C, Eicken, H, Polashenski, CM, Sturm, M, Harbeck, JP, Perovich, DK, Finnegan, DC. 2012. Snow dunes: A controlling factor of melt pond distribution on Arctic sea ice. *Journal of Geophysical Research* **117**: C09029. DOI: http://dx.doi.org/10.1029/2012JC008192.

Platt, T, Gallegos, CL, Harrison, WG. 1980. Photoinhibition of photosynthesis in natural assemblages of marine phytoplanton. *Journal of Marine Research* **38**(4): 687–701.

Poulin, M, Daugbjerg, N, Gradinger, R, Ilyash, L, Ratkova, T, Quillf, C. 2011. The pan-Arctic biodiversity of marine pelagic and sea-ice unicellular eukaryotes: a first-attempt assessment. *Marine Biodiversity* **41**: 13–28. DOI: http://dx.doi.org/10. 1007/s12526-010-0058-8.

Pućko, M, Dionne, K, Michel, C. 2019. Occurrence of toxin-producing marine algae in the Canadian Arctic and adjacent waters. *Canadian Manuscript Report of Fisheries and Aquatic Sciences* **3180**(vii): 27.

Raymond, JA. 2011. Algal ice-binding proteins change the structure of sea ice. *PNAS* **108**(24): E198. DOI: http://dx.doi.org/10.1073/pnas.1106288108.

Richardson, K, Beardall, J, Raven, JA. 1983. Adaptation of unicellular algae to irradiance: An analysis of strategies. *New Phytology* **93**: 157–191.

Riedel, A, Michel, C, Gosselin, M. 2006. Seasonal study of sea-ice exopolymeric substances on the Mackenzie shelf: implications for transport of sea-ice bacteria and algae. *Aquatic Microbial Ecology* **45**(2): 195–206. DOI: http://dx.doi.org/10.3354/ame045195.

Różańska, M, Gosselin, M, Poulin, M, Wiktor, JM, Michel, C. 2009. Influence of environmental factors on the development of bottom landfast ice protists in the Canadian Beaufort Sea during the winter-spring transition. *Marine Ecology Progress Series* **386**: 43–59. DOI: http://dx.doi.org/10.3354/meps08092.

Rysgaard, S, Glud, RN. 2004. Anaerobic N_2 production in Arctic sea ice. *Limnology and Oceanography* **49**(1): 86–94. DOI: http://dx.doi.org/10.4319/lo.2004.49.1.0086.

Rysgaard, S, Glud, RN, Sejr, MK, Blicher, ME, Stahl, HJ. 2008. Denitrification activity and oxygen dynamics in Arctic sea ice. *Polar Biology* **31**: 527–537. DOI: http://dx.doi.org/10.1007/s00300-007-0384-x.

Rysgaard, S, Kuhl, M, Hansen, JW. 2001. Biomass, production and horizontal patchiness of sea ice microalgae in a High-Arctic fjord (Young Sound, NE Greenland). *Marine Ecology Progress Series* **223**: 15–26. DOI: http://dx.doi.org/10.3354/meps223015.

Schünemann, H, Werner, I. 2005. Seasonal variations in distribution patterns of sympagic meiofauna in Arctic pack ice. *Marine Biology* **146**(6): 1091–1102. DOI: http://dx.doi.org/10.1007/s00227-004-1511-7.

Smith, REH, Herman, AW. 1991. Productivity of sea ice algae: In situ vs. incubator methods. *Journal of Marine Systems* **2**: 97–110.

Søgaard, DH, Kristensen, M, Rysgaard, S, Glud, RN, Hansen, PJ, Hilligsøe, KM. 2010. Autotrophic and heterotrophic activity in Arctic first year sea ice: seasonal study from Malene Bight, SW Greenland. *Marine Ecology Progress Series* **419**: 31–45. DOI: http://dx.doi.org/10.3354/meps08845.

Søgaard, DH, Sorell, BH, Sejr, MK, Andersen, P, Rysgaard, S, Hansen, PJ, Skyttä, A, Lemcke, S, Lund-Hansen, C. 2021. An under-ice bloom of mixotrophic haptophytes in low nutrient and freshwater-influenced Arctic waters. *Scientific Reports* **11**: 2915. DOI: http://dx.doi.org/10.1038/s41598-021-82413-y.

Sorrell, BK, Hawes, I, Stratmann, T, Lund-Hansen, LC. 2021. Photobiological effects on ice algae of a rapid whole-fjord loss of snow cover during spring growth in Kamgerlussuag, a West Greenland fjord. *Journal of Marine Science and Engineering* **9**(814): 814. DOI: http://dx.doi.org/10.3390/jmse9080814

Strickland, JDH, Parsons, TR. 1972. *A practical handbook of seawater analysis*. Ottawa, Canada: Fisheries Board of Canada.

Stroeve, JC, Markus, T, Boisvert, L, Miller, J, Barrett, A. 2014. Changes in Arctic melt season and implications for sea ice loss. *Geophysical Research Letters* **41**: 1216–1225. DOI: http://dx.doi.org/10.1002/2013GL058951.

Stroeve, JC, Vancoppenolle, M, Veyssière, G, Lebrun, M, Castellani, G, Babin, M, Karcher, M, Landy, J, Liston, GE, Wilkinson, J. 2021. A multi-sensor and modeling approach for mapping light under sea ice during the ice-growth season. *Frontiers in Marine Science* **7**. DOI: http://dx.doi.org/10.3389/fmars.2020.592337.

Tremblay, J, Anderson, LG, Matrai, P, Coupel, P, Bélanger, S, Michel, C, Reigstad, M. 2015. Global and regional drivers of nutrient supply, primary production and CO_2 drawdown in the changing Arctic Ocean. *Progress in Oceanography* **139**: 171–196. DOI: http://dx.doi.org/10.1016/j.pocean.2015.08.009.

Tschudi, MA, Meier, W, Stewart, JS. 2020. An enhancement to sea ice motion and age products at the National Snow and Ice Data Centre (NSIDC). *The Cryosphere* **14**: 1519–1536. DOI: http://dx.doi.org/10.5194/tc-14-1519-2020

Underwood, GJC, Aslam, SN, Michel, C, Niemi, A, Norman, L, Meiners, KM, Laybourn-Parry, JL, Patersong, H, Thomas, DN. 2013. Broad-scale predictability of carbohydrates and exopolymers in Antarctic and Arctic sea ice. *Proceedings in the National Academy of Sciences* **110**(39): 15734–15739. DOI: http://dx.doi.org/10.1073/pnas.1302870110.

Underwood, GJC, Michel, C, Meisterhans, G, Niemi, A, Belzile, C, Witt, M, Dumbrell, AJ, Koch, BP. 2019. Organic matter from melting Arctic sea ice alters bacterial community structure and function. *Nature Climate Change* **9**: 170–176. DOI: http://dx.doi.org/10.1038/s41558-018-0391-7.

Underwood GJC, Paterson, DM. 2003. The importance of extracellular carbohydrate production by marine epipelic diatoms. *Advances in Botany Research* **40**: 183–240. DOI: http://dx.doi.org/10.1016/S0065-2296(05)40005-1.

Vihma, T. 2014. Effects of Arctic sea ice decline on weather and climate: A review. *Surveys in Geophysics* **35**: 1175–1214. DOI: http://dx.doi.org/10.1007/s10712-014-9284-0.

Wang, S, Bailey, D, Lindsay, K, Moore, JK, Holland, M. 2014. Impact of sea ice on the marine iron cycle and phytoplankton productivity. *Biogeosciences* **11**: 4713–4731. DOI: http://dx.doi.org/10.5194/bg-11-4713-2014.

Webster, M, Gerland, S, Holland, M, Hunke, E, Kwok, R, Lecomte, O, Massom, R, Perovich, D, Sturm, M. 2018. Snow in the changing sea-ice systems. *Nature Climate Change* **8**(11): 946–953. DOI: http://dx.doi.org/10.1038/s41558-018-0286-7.

Wongpan, P, Meiners, KM, Langhorne, PJ, Heil, P, Dmith, IJ, Leonard, GH, Massom, RA, Clementson, LA, Haskell, TG. 2018. Estimation of Antarctic land-fast sea ice algal biomass and snow thickness from under-ice radiance spectra in two contrasting areas. *Journal of Geophysical Research: Oceans* **123**, 1907–1923. DOI: http://dx.doi.org/10.100272017JC013711.

Wongpan, P, Nomura, D, Toyota, T, Tanikawa, T, Meiners, K, Ishino, T, Tamura, TP, Tozawa, M, Nosaka, Y, Hirawake, T, Ooki, A, Shigeru, A. 2020. Using under-ice hyperspectral transmittance to determine land-fast sea-ice algal biomass in Saroma-ko Lagoon, Hokkaido, Japan. *Annals Glaciology* **61**(82): 1–10. DOI: http://dx.doi.org/10.1017/aog.2020.69.

How to cite this article: Campbell, K, Lange, BA, Landy, JC, Katlein, C, Nicolaus, M, Anhaus, P, Matero, I, Gradinger, R, Charette, J, Duerksen, S, Tremblay, P, Rysgaard, S, Tranter, M, Haas, C, Michel, C. 2021. Net heterotrophy in High Arctic first-year and multi-year spring sea ice. *Elementa: Science of the Anthropocene* 10(1). DOI: https://doi.org/10.1525/elementa.2021.00040

Domain Editor-in-Chief: Jody W. Deming, University of Washington, Seattle, WA, USA

Associate Editor: Kevin R. Arrigo, Department of Earth System Science, Stanford University, Stanford, CA, USA

Knowledge Domain: Ocean Science

Part of an Elementa Special Feature: Multidisciplinary Arctic Program—Last Ice

Published: January 4, 2022 **Accepted:** October 25, 2021 **Submitted:** June 1, 2021

ELEMENTA Science of the Anthropocene

Elem Sci Anth is a peer-reviewed open access journal published by University of California Press.

OPEN ACCESS